Check for updates

International Journal of Robust and Nonlinear Control

WILEY

RESEARCH ARTICLE

Event-Triggered Adaptive Asymptotic Tracking Control for Stochastic Non-Linear Systems With Unknown Hysteresis: A New Switching Threshold Approach

Yang Du[1,2] | Wei Zhao[1,2] | Shan-Liang Zhu[1,2,3] | Wei-Jie Hao[1,2] | Shi-Cheng Liu[1,2] | Yu-Qun Han[1,2,3]

[1]School of Mathematics and Physics, Qingdao University of Science and Technology, Qingdao, China | [2]Qingdao Innovation Center of Artificial Intelligence Ocean Technology, Qingdao, China | [3]Research Institute for Mathematics and Interdisciplinary Sciences, Qingdao University of Science and Technology, Qingdao, China

Correspondence: Yu-Qun Han (yuqunhan@163.com)

Received: 16 February 2024 | **Revised:** 1 October 2024 | **Accepted:** 15 December 2024

Funding: This research was supported by the Shandong Provincial Natural Science Foundation, China (No. ZR2020QF055).

Keywords: asymptotic tracking control | bounded estimation method | event-triggered control | multi-dimensional Taylor network | stochastic non-linear systems

ABSTRACT

This paper proposes a novel event-triggered adaptive asymptotic tracking control (ATC) method for stochastic non-linear systems with unknown hysteresis. Firstly, in order to reduce the depletion of network resources while optimizing the asymptotic tracking performance of the system, a switching threshold mechanism (STM)-based event-triggered control (ETC) strategy is adopted. Secondly, a first-order filter is utilized to address the problem of the contradiction between event-triggered mechanism (ETM) output and rate-dependent hysteresis actuator input. By incorporating an enhanced backstepping technique and a bounded estimation method, it is rigorously demonstrate that the system achieves zero tracking error, effectively compensates for unknown hysteresis, and ensures that all closed-loop signals remain bounded in probability. Meanwhile, the Zeno phenomenon is excluded. Finally, the effectiveness and superiority of the proposed control scheme are verified by the simulation results.

1 | Introduction

With the increasing accuracy of the systems under consideration, the factor of stochastic disturbances becomes non-negligible. Hence, it is of great practical importance to study various control approaches for stochastic non-linear systems, such as adaptive backstepping control [1, 2], Lyapunov function approach [3] and robust control [4]. Among them, adaptive backstepping control has emerged as a powerful technique to solve control problems of uncertain non-linear stochastic systems. In addition, fuzzy logic systems (FLSs) [5, 6], neural networks (NNs) [7–9] and multi-dimensional Taylor network (MTN) [10–13] control have also become effective control methods to compensate for the effects of unknown uncertainties and strong non-linearities. While these control schemes can limit the tracking error to the vicinity of the origin by adjusting design parameters, they still cannot guarantee zero tracking error in the system output. Thereby, the research focus has been shifted to asymptotic tracking control (ATC) [14, 15]. Nevertheless, the local controllers developed in the above-mentioned literature operate continuously, which may lead to unnecessary communication traffic and computational difficulties.

© 2025 John Wiley & Sons Ltd.

https://doi.org/10.1002/rnc.7799

Over the past few decades, multiple types of event-triggered mechanisms (ETMs) have been reported. For example, fixed threshold mechanism (FTM)-based event-triggered control (ETC) strategy was applied in consensus control of multi-intelligent systems and output feedback control of micro-electromechanical system gyroscope in [16] and [17]. It is worth noting that such static ETM may result in conservative estimates for the number of event-trigger, potentially leading to suboptimal control performance. In this case, some ETMs based on time-varying thresholds were further developed in [18–21]. For example, different ETMs with dynamic relative thresholds were used for adaptive fixed-time control of non-strict feedback systems and scheduling stabilization control tasks for non-affine systems in [18] and [21]. In [22] and [23], two novel dynamic ETMs were designed to address the problem of disturbance rejection control and fault detection in networked control systems, respectively. However, it is worth pointing out that strong signal impulses may be applied to the systems under these dynamic ETMs, affecting the tracking performance [24]. Based on the above discussion, the ingenious combination of the above ETMs will bring the possibility to further optimize the asymptotic tracking performance realized in [25–28]. Therefore, the motivation of the current research is to develop an intelligent switching threshold mechanism (STM) that automatically identifies the amplitude of the control signal, enabling continuous switching between dynamic relative threshold mechanisms (RTM) and FTM.

In addition to the influence of the aforementioned ETMs on system tracking performance, actuator non-linearity also inevitably affects system performance, such as hysteresis [29–31], saturation [32, 33] and dead-zone [34–37]. Among them, actuator hysteresis, as a significant non-smooth non-linearity, has attracted extensive attention of scholars and numerous control schemes have been developed to compensate for various types of hysteresis for diverse non-linear systems, such as switched stochastic pure-feedback systems [38], multi-agent systems [39, 40] and non-linear time-varying delay systems [41]. Notably, a novel adaptive ATC method for stochastic non-linear systems with backlash-like hysteresis was proposed in [42] and by introducing ETC strategy, an adaptive leaderless consensus control was studied in [43] for non-linear multi-agent systems with unknown hysteresis. However, the research [44–46] shows that hysteresis is rate-dependent, which means that the shape of hysteresis will be affected by the input signal rate. For this reason, discrete signals generated by ETMs cannot be directly applied as inputs to hysteresis actuators, posing an additional challenge in designing controllers that effectively compensate for hysteresis.

Based on the above statements, an adaptive ATC problem for a class of stochastic non-linear systems with unknown hysteresis is considered, which uses the MTN approximation method, Nussbaum function, adaptive backstepping technique, ETC strategy, and bounded estimation method. In short, our contributions include four aspects.

1. For a class of stochastic non-linear systems with unknown hysteresis, an event-triggered adaptive MTN asymptotic tracking controller with strong performance and the lower energy consumption is designed, which can not only compensate for stochastic disturbances and unknown hysteresis, but also ensure that the system output with zero tracking error.
2. A universal first-order filter is innovatively employed to ensure that the discrete control signals generated by the ETM are smooth and differentiable, thereby resolving the conflict with the input rate-dependence of the hysteresis actuator. However, the introduction of this first-order filter results in the generation of an additional state, rendering the conventional n-step backstepping design unsuitable. Consequently, this paper proposes an improved backstepping design method to address this issue.
3. Compared to the RTM-based event-triggered ATC methods reported in [25–28], this paper introduces an intelligent switching ETM, aiming to further optimize the asymptotic tracking performance of the system by maintaining the regular operation of the system components. Although the STM has been discussed in [24], its application to stochastic non-linear systems remains unexplored. This mechanism enhances the system's robustness against stochastic disturbances and internal uncertainties, enabling the system to sustain stable performance across diverse operating conditions, thereby ensuring the efficacy of the control strategy.
4. For the first time, this paper considers unknown actuator hysteresis, event-triggered control, and adaptive tracking control within a unified theoretical framework for stochastic non-linear systems. It is worth pointing out that event-triggered ATC methods have been reported in [25–28]. However, the controlled systems are diverse non-linear systems rather than stochastic non-linear systems with unknown hysteresis. Even though the ATC strategy for stochastic non-linear systems with unknown hysteresis has been proposed in [42], the problem of limited network resources cannot be solved. Therefore, the systems and problems considered in this paper are more comprehensive.

2 | Problem Statement and Some Preliminaries

Notations:

a. R, R^n and R^+ represent the set of all non-negative real numbers, the real n-dimensional vector space, and the set of all non-negative real numbers, respectively. In addition, $R^{n\times r}$ represents the real $n \times r$ matrix space.

b. $C^{2,1}$ denotes the sets of all non-negative functions $V(x,t)$, which are C^2 in x and C^1 in t, where C^i represents the set of all functions with continuous i-th partial derivatives.

c. For a given vector or matrix H, $\mathrm{Tr}\{H\}$ and H^{T} represent its trace (when H is square matrix) and its transpose, respectively.

2.1 | Problem Statement

Considering the stochastic non-linear system with unknown hysteresis as follows

10991239, 2025, 6, Downloaded from https://onlinelibrary.wiley.com/doi/10.1002/rnc.7799 by QINGDAO UNIVERSITY OF SCIENCE & TECH, Wiley Online Library on [04/03/2026]. See the Terms and Conditions (https://onlinelibrary.wiley.com/terms-and-conditions) on Wiley Online Library for rules of use; OA articles are governed by the applicable Creative Commons License

$$\begin{cases} dx_i = \left(f_i\left(\overline{\boldsymbol{x}}_i\right) + x_{i+1}\right)dt + h_i^{\mathrm{T}}\left(\overline{\boldsymbol{x}}_i\right)d\boldsymbol{\omega} \\ i = 1, 2, \ldots, n-1 \\ dx_n = \left(f_n\left(\overline{\boldsymbol{x}}_n\right) + H(\vartheta)\right)dt + h_n^{\mathrm{T}}\left(\overline{\boldsymbol{x}}_n\right)d\boldsymbol{\omega} \\ y = x_1 \end{cases} \tag{1}$$

where $\overline{\boldsymbol{x}_i} = [x_1, x_2, \ldots, x_i]^{\mathrm{T}} \in R^i, i = 1, 2, \ldots, n$ is the state vector of the system. $H(\vartheta) : R \to R$ and $y \in R$ represent the system input signal and output signal, respectively. Especially, the system input signal $H(\vartheta)$ is subjected to the unknown hysteresis non-linearity, which will be given later. $f_i(\cdot) : R^i \to R$ and $h_i(\cdot) : R^i \to R$ are the unknown smooth non-linear functions and satisfy $f_i(\mathbf{0}) = 0$, $h_i(\mathbf{0}) = 0$; $\boldsymbol{\omega}$ is a standard Wiener process.

For system (1) with unknown hysteresis, the objectives of the proposed control strategy in this paper include the following three aspects:

a. For a given reference signal y_d, the tracking error $y - y_d$ converges to a small neighbourhood of zero.

b. All closed-loop signals are bounded in probability on $[0, +\infty)$.

c. There is no Zeno phenomenon.

Assumption 1. The given reference signal y_d is continuously differentiable and bounded, and its i-th time derivative $y_d^{(i)}$ is also continuously differentiable and bounded, where $i = 1, 2, \ldots, n+1$.

Remark 1. It is worth noting that Assumption 1 is a normal assumption for non-linear systems [10, 13] which ensures the feasibility of controller design.

To reduce the depletion of network resources, an emerging STM about ETC is co-designed with an adaptive controller.

$$\vartheta(t) = \varpi\left(t_k\right), \forall t \in \left[t_k, t_{k+1}\right) \tag{2}$$

$$t_{k+1} = \begin{cases} \inf\{t \in R : |e(t)| \geq m\}, |\vartheta(t)| > \hbar \\ \inf\left\{r \in R : |e(t)| \geq \varsigma|\vartheta(t)| + m_1\right\}, |\vartheta(t)| \leq \hbar \end{cases} \tag{3}$$

where $\hbar$, $0 < \varsigma < 1$, t_k, $k \in Z^+$, m, m_1 are known positive design parameters; t_k is the controller update moment; whenever (3) is triggered, we mark the time as t_{k+1} and the controller's output $\vartheta\left(t_{k+1}\right)$ will be applied to the actuator; from (2), during the time $t \in \left[t_k, t_{k+1}\right)$, the actuator's input value $\vartheta(t)$ will remain unchanged as a constant $\vartheta\left(t_k\right)$; $e(t) = \varpi(t) - \vartheta(t)$ stands for the measurement error.

For emerging STM, the following definition is given to facilitate the design of subsequent event-triggered controller

$$e_1 = \max\left\{\varsigma\hbar + m_1, m\right\} \tag{4}$$

2.2 | Stochastic Stability

To elaborate on the definition of a stochastic non-linear system, the general form of the system can be expressed as

$$d\boldsymbol{x}(t) = f(\boldsymbol{x}, t)dt + h(\boldsymbol{x}, t)d\boldsymbol{\omega} \tag{5}$$

where $\boldsymbol{x} \in R^n$ is the system state vector; $\boldsymbol{\omega}$ is an r-dimensional standard Wiener process; the local Lipschitz functions $f(\boldsymbol{x}, t) \in R^n$ and $h(\boldsymbol{x}, t) \in R^{n\times r}$ satisfy conditions that $f(\mathbf{0}, t) = \mathbf{0}$ and $h(\mathbf{0}, t) = \mathbf{0}$, respectively.

Definition 1. ([37, 47]). For any function $V(\boldsymbol{x}, t) \in C^{2,1}$ associated with system (5), the differential operator L is defined as follows

$$LV(\boldsymbol{x}, t) = \frac{\partial V(\boldsymbol{x}, t)}{\partial t} + \frac{\partial V(\boldsymbol{x}, t)}{\partial x} f + \frac{1}{2}\mathrm{Tr}\left\{h^{\mathrm{T}}\frac{\partial^2 V(\boldsymbol{x}, t)}{\partial x^2}h\right\} \tag{6}$$

Lemma 1. ([37]). *If there exists a function $V(\boldsymbol{x}, t) \in C^2$, for all $x \in R^n$ and $t > t_0$, one has*

$$\begin{cases} \wp_1(|\boldsymbol{x}|) \leq V(\boldsymbol{x}, t) \leq \wp_2(|\boldsymbol{x}|) \\ LV(\boldsymbol{x}, t) \leq -c_1 V(\boldsymbol{x}, t) + c_2 \end{cases} \tag{7}$$

where $\wp_1(\cdot)$ and $\wp_2(\cdot)$ are class $K\infty$-functions, and $c_1 > 0$, $c_2 > 0$ are constants. Then, for each $x_0 \in R^n$, the system (5) has a unique strong solution, and all its states are bounded.

2.3 | Hysteresis Characteristic

As stated in [41], the system input signal $H(\vartheta)$ can be expressed as the following Bouc–Wen hysteresis non-linearity

$$\dot{\xi} = \mathrm{A}\dot{\vartheta} - \gamma|\dot{\vartheta}|\xi|\xi|^{n-1} - \beta\dot{\vartheta}|\xi|^n \tag{8}$$

$$H(\vartheta) = \rho_1\vartheta + \rho_2\xi \tag{9}$$

where A is the restoring force amplitude control parameter and satisfies $\mathrm{A} = 1$; ϑ and $H(\vartheta)$ represent the hysteresis input and output, respectively; $n > 1$ affects the smoothness of the transition from the initial slope to the asymptotic slope; $\gamma \geq |\beta|$, γ and β are control parameters that describe the shape and amplitude of hysteresis; ρ_1 and ρ_2 as constants represent the control direction of the hysteresis and satisfy $sign\left(\rho_1\right) = sign\left(\rho_2\right)$; the auxiliary variable $\xi(t)$ satisfies $|\xi(t)| \leq \sqrt[n]{\frac{1}{\gamma+\beta}}$, and $\xi\left(t_0\right) = 0$.

Assumption 2. The $sign\left(\rho_1\right)$ is unknown and satisfies $0 \leq \underline{\rho}_1 \leq |\rho_1| \leq \overline{\rho}_1$, $|\rho_1| \neq 0$, $\underline{\rho}_1$ and $\overline{\rho}_1$ are constants.

Remark 2. Since the actual engineering environment is complex, unlike the hysteresis phenomenon concerned in [29, 30], the control direction ρ_1 studied in this paper is unknown.

2.4 | Nussbaum-Type Function

If there exists a function $N(\eta)$ that satisfies the following two given properties, then it is named as Nussbaum-type function.

$$\lim_{\kappa\to\pm\infty}\sup\frac{1}{\kappa}\int_0^{\kappa} N(\eta)d\eta = +\infty \tag{10}$$

$$\lim_{\kappa\to\pm\infty}\inf\frac{1}{\kappa}\int_0^{\kappa} N(\eta)d\eta = -\infty \tag{11}$$

10991239, 2025, 6, Downloaded from https://onlinelibrary.wiley.com/doi/10.1002/rnc.7799 by QINGDAO UNIVERSITY OF SCIENCE & TECH, Wiley Online Library on [04/03/2026]. See the Terms and Conditions (https://onlinelibrary.wiley.com/terms-and-conditions) on Wiley Online Library for rules of use; OA articles are governed by the applicable Creative Commons License

It should be noted that there are many functions with the above properties, such as $\eta^2\cos(\eta)$, $e^{\eta^2}\cos(\eta)$, e^{η^2} and $\eta^2\sin(\eta)$.

Lemma 2. ([37]). *Considering the stochastic system (5), assume that there exists a function $V(\boldsymbol{x},t)$ with the same definition as in Definition 1, the smooth function $\eta(t): R^+ \to R$, the bounded function $\phi(\boldsymbol{x},t)$ and the Nussbaum-type function $N(\eta)$ are all defined in $[0,t_f)$; $\psi>0$ and $b>0$ are random variables, $M(t)$ is a real valued continuous local martingale and satisfies condition $M(0)=0$ such that*

$$V(\boldsymbol{x},t) \le \psi + e^{-bt}\int_0^t (\phi(\boldsymbol{x},t)N(\eta)+1)\dot{\eta}e^{b\sigma}d\sigma + M(t) \quad \forall t\in[0,t_f) \tag{12}$$

Then, for $x_0\in R^n$, the following functions $\eta(t)$, $V(\boldsymbol{x},t)$ and $\int_0^t(\phi(\boldsymbol{x},t)N(\eta)+1)\dot{\eta}d\sigma$ are bounded in probability on $[0,t_f)$. Furthermore, it follows from Proposition 2 in [36] that $t_f\to\infty$ when the solution of the closed-loop system is bounded.

2.5 | MTN and Necessary Lemmas

In this paper, MTNs are used to approximate unknown non-linearities that arise during the controller design process. MTN is a three-layer neural network with a special structure, its structural diagram is shown in Figure 1. Especially, the approximation principle of the MTN is described as follows.

Lemma 3. ([10, 11, 48]). *Given a continuous and unknown function $\mathrm{T}(Z)$ defined on a compact set $\mathrm{X}\in R^n$, for $\forall\varepsilon>0$, there exist an MTN denoted as $\boldsymbol{\varphi}^{\mathrm{T}}\mathrm{P}_{m_n}(Z)$ satisfying the following expression*

$$\mathrm{T}(Z) = \boldsymbol{\varphi}^T\mathrm{P}_{m_n}(Z)+\delta(Z), |\delta(Z)|\le\varepsilon \tag{13}$$

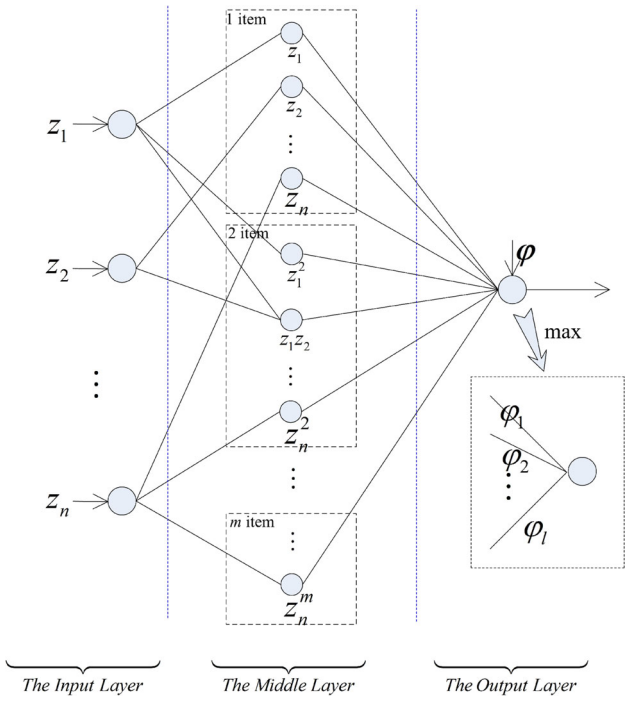

FIGURE 1 | The structural diagram of MTN.

where $Z=[z_1,\ldots,z_n]^{\mathrm{T}}\in\mathrm{X}\subset R^n$ is the input vector of MTN, $\mathrm{P}_{m_n}(Z)=[z_1,\ldots,z_n,z_1^2,z_1z_2,\ldots,z_1z_n,z_2z_3,\ldots,z_n^2,z_1^m,\ldots,z_n^m]^{\mathrm{T}}\in R^l$ stands for the intermediate input layer of MTN and $\boldsymbol{\varphi}=[\varphi_1,\ldots,\varphi_l]^{\mathrm{T}}\in R^l$ denotes the weight vector of MTN. $\delta(Z)$ represents the error of MTN in approximation.

Remark 3. As a network structure similar to a radial basis function neural network (RBFNN), the MTN consists of three layers: an input layer, a middle layer, and an output layer. Unlike the middle layer of an RBFNN, the MTN is composed of a set of polynomials instead of Gaussian functions, effectively simplifying the RBFNN structure and reducing computational complexity.

In addition, the following two lemmas will be used in the controller design process.

Lemma 4. ([14]). *For a given bounded and continuous function $\upsilon(t)>0$ and $\tau\in R$, the following inequality is true*

$$|\tau| \le \frac{\tau^2}{\sqrt{\tau^2+\upsilon^2(t)}} + \upsilon(t) \tag{14}$$

where $\upsilon(t)$ satisfies $\lim_{t\to+\infty}\int_{t_0}^t\upsilon(s)ds\le\bar{\upsilon}<+\infty$ and $\bar{\upsilon}>0$ is a constant.

Lemma 5. ([18]). *Given a continuous function $\zeta(t)>0,\forall t\ge 0$ and $\Psi>0$, the following property holds*

$$0\le|\Psi|-\Psi\tanh\left(\frac{\Psi}{\zeta(t)}\right)\le 0.2785\zeta(t) \tag{15}$$

3 | Controller Design and Stability Analysis

3.1 | Event-Triggered Asymptotic Controller Design

In this subsection, a novel adaptive MTN controller via combining ETM and bounded estimation method is designed.

To reduce the depletion of network resources, an event-triggered controller is designed, which will result in discrete control output signals. However, the Bouc–Wen hysteresis phenomenon considered in this paper is input rate-dependent, which will lead to conflicting control design of the system. Therefore, to solve the above problem, a first-order filter is used to generate a smooth and differentiable signal to act on the input of the hysteresis actuator, as shown in Figure 2.

For the stochastic systems, the first-order filter has the following form

$$d\vartheta_s = \big(b(\vartheta-\vartheta_s)\big)dt \tag{16}$$

where ϑ_s and b represent the accessible state and output, and the control coefficient of the filter, respectively.

By introducing the first-order filter, the system (1) can be represented as

10991239, 2025, 6, Downloaded from https://onlinelibrary.wiley.com/doi/10.1002/rnc.7799 by QINGDAO UNIVERSITY OF SCIENCE & TECH, Wiley Online Library on [04/03/2026]. See the Terms and Conditions (https://onlinelibrary.wiley.com/terms-and-conditions) on Wiley Online Library for rules of use; OA articles are governed by the applicable Creative Commons License

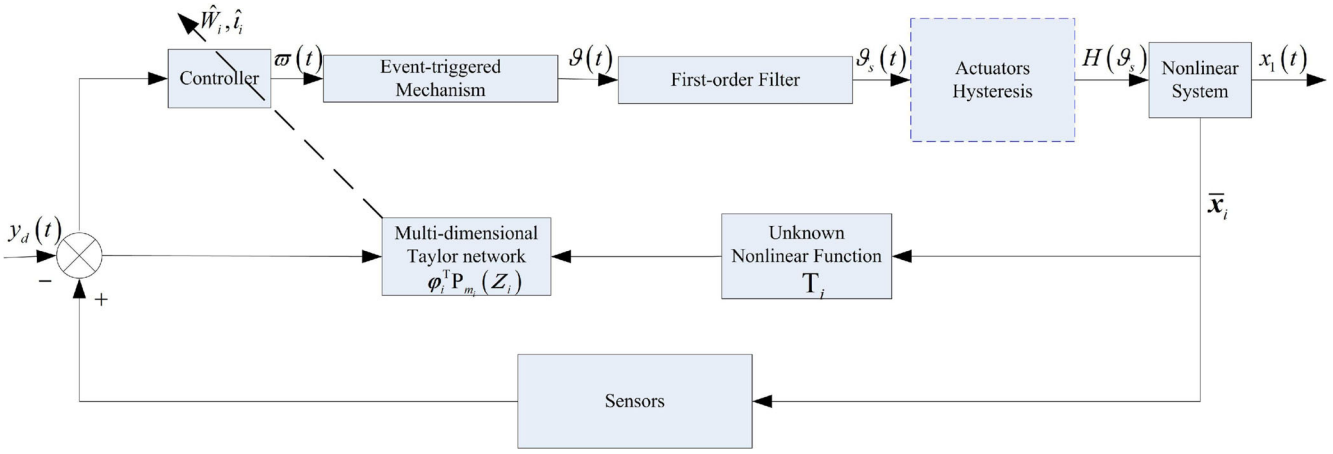

FIGURE 2 | The control flow of the proposed strategy.

$$\begin{cases} dx_i = \left(f_i(\bar{x}_i) + x_{i+1}\right)dt + h_i^{\mathrm{T}}(\bar{x}_i)d\boldsymbol{\omega} \\ i = 1, 2, \ldots, n-1 \\ dx_n = \left(f_n(\bar{x}_n) + H(\vartheta_s)\right)dt + h_n^{\mathrm{T}}(\bar{x}_n)d\boldsymbol{\omega} \\ H(\vartheta_s) = \rho_1\vartheta_s + \rho_2\xi \\ d\vartheta_s = \left(b(\vartheta - \vartheta_s)\right)dt \\ y = x_1 \end{cases} \tag{17}$$

Remark 4. Due to the introduction of the first-order filter, an additional state ϑ_s is added, which will make the design of the control system more difficult. To address the effect of the added state ϑ_s in the control design process, a novel backstepping design with $n+1$ steps is proposed.

Based on the backstepping technique, we define the corresponding coordinate transformations as follows

$$\begin{cases} z_1 = x_1 - y_d \\ z_i = x_i - \alpha_{i-1}, i = 2, \ldots, n \\ z_{n+1} = \vartheta_s - \alpha_n \end{cases} \tag{18}$$

where $\alpha_i, i = 1, \ldots, n$ denotes the virtual control law, and $z_i, i = 1, \ldots, n+1$ is the error variable.

The unknown parameters in this paper will be disposed of via using the bounded estimation method, therefore, we need to have the following definition.

$$W_i = \|\boldsymbol{\varphi}_i\|, \iota_i = \varepsilon_i + \frac{3}{2}|\Phi_i|, i = 1, 2, \ldots, n+1 \tag{19}$$

$$\tilde{W}_i = W_i - \hat{W}_i, \tilde{\iota}_i = \iota_i - \hat{\iota}_i \tag{20}$$

where $\tilde{W}_i$ and $\tilde{\iota}_i$ represent the parameter errors W_i and ι_i, respectively, and Φ_i will be defined in Lemma 6.

Lemma 6. ([49]). *For the non-linear functions* $\Xi_i = \frac{z_i^3 \mathrm{P}_{m_i}^T \mathrm{P}_{m_i}}{\sqrt{z_i^6 \mathrm{P}_{m_i}^T \mathrm{P}_{m_i} + \upsilon_i^2}}$ *and* $\Phi_i = \frac{z_i \mathrm{H}_i^2}{\sqrt{z_i^4 \mathrm{H}_i^2 + \upsilon_i^2}}, i = 1, 2, \ldots, n+1$, *we get*

$$z_i^3 \boldsymbol{\varphi}_i^T \mathrm{P}_{m_i} \le W_i z_i^3 \Xi_i + W_i \upsilon_i \tag{21}$$

$$z_i^2 \mathrm{H}_i \le z_i^3 \Phi_i + \upsilon_i \tag{22}$$

where H_i *will be defined later*.

Step 1: According to (17) and (18), we obtain the derivative of z_1 as

$$dz_1 = \left(x_2 + f_1 - \dot{y}_d\right)dt + h_1^{\mathrm{T}} d\boldsymbol{\omega} \tag{23}$$

To achieve ATC, the following first Lyapunov function is chosen

$$V_1 = \frac{1}{4}z_1^4 + \frac{1}{2}\tilde{W}_1^2 + \frac{1}{2}\tilde{\iota}_1^2 \tag{24}$$

where $\tilde{W}_1$ and $\tilde{\iota}_1$ are defined in (20).

By using Definition 1 on (23) and (24), we get

$$LV_1 = z_1^3\left(\left(z_2 + \alpha_1\right) + f_1 - \dot{y}_d\right) + \frac{3}{2}z_1^2 \mathrm{H}_1 - \tilde{W}_1\dot{\hat{W}}_1 - \tilde{\iota}_1\dot{\hat{\iota}}_1 \tag{25}$$

where $\mathrm{H}_1 = \|h_1\|^2$.

Then, by using Young's Inequality and Lemma 6, the following two inequalities are obtained

$$z_1^3 z_2 \le \frac{3}{4}z_1^4 + \frac{1}{4}z_2^4 \tag{26}$$

$$\frac{3}{2}z_1^2 \mathrm{H}_1 \le \frac{3}{2}z_1^3 \Phi_1 + \frac{3}{2}\upsilon_1 \tag{27}$$

By combining (26) and (27), (25) can be rewritten as

$$LV_1 \le z_1^3\left(\alpha_1 + \mathrm{T}_1 + \frac{3}{2}\Phi_1\right) + \frac{1}{4}z_2^4 + \frac{3}{2}\upsilon_1 - \tilde{W}_1\dot{\hat{W}}_1 - \tilde{\iota}_1\dot{\hat{\iota}}_1 \tag{28}$$

where $\mathrm{T}_1 = f_1 - \dot{y}_d + \frac{3}{4}z_1$. It is easy to see that T_1 in (28) is an unknown smooth non-linear function, so for $\forall\varepsilon_1 > 0$, there exists an MTN that is used to approximate it as follows

$$\mathrm{T}_1 = \boldsymbol{\varphi}_1^{\mathrm{T}} \mathrm{P}_{m_1}(Z_1) + \delta(Z_1), \left|\delta_1(Z_1)\right| \le \varepsilon_1 \tag{29}$$

where $Z_1 = [z_1, y_d, \dot{y}_d]^{\mathrm{T}}$ and $\delta_1(Z_1)$ represent the input vector and the approximation error of MTN, respectively.

10991239, 2025, 6, Downloaded from https://onlinelibrary.wiley.com/doi/10.1002/rnc.7799 by QINGDAO UNIVERSITY OF SCIENCE & TECH, Wiley Online Library on [04/03/2026]. See the Terms and Conditions (https://onlinelibrary.wiley.com/terms-and-conditions) on Wiley Online Library for rules of use; OA articles are governed by the applicable Creative Commons License

According to (19) and (29), and using Lemma 6, we get

$$\begin{aligned} z_1^3\left(\mathrm{T}_1+\frac{3}{2}\Phi_1\right) =& z_1^3\left(\varphi_1^{\mathrm{T}}\mathrm{P}_{m_1}(Z_1)+\delta(Z_1)+\frac{3}{2}\Phi_1\right)W_1 z_1^3\Xi_1 \\ &+W_1\upsilon_1+\left|z_1^3\right|\left(\varepsilon_1+\frac{3}{2}|\Phi_1|\right) \\ =& W_1 z_1^3\Xi_1+W_1\upsilon_1+\left|z_1^3\right|\iota_1 \end{aligned} \tag{30}$$

Then, using the Lemma 4, we can further get the following inequality

$$\left|z_1^3\right|\iota_1 \le \frac{\iota_1 z_1^6}{\sqrt{z_1^6+\upsilon_1^2}}+\iota_1\upsilon_1 \tag{31}$$

By combining (30) and (31), (28) can be expressed as

$$\begin{aligned} LV_1 \le & z_1^3\alpha_1+\hat{W}_1 z_1^3\Xi_1+\frac{\hat{\iota}_1 z_1^6}{\sqrt{z_1^6+\upsilon_1^2}}-\tilde{W}_1\left(\dot{\hat{W}}_1-z_1^3\Xi_1\right) \\ &-\tilde{\iota}_1\left(\dot{\hat{\iota}}_1-\frac{z_1^6}{\sqrt{z_1^6+\upsilon_1^2}}\right)+\left(W_1+\iota_1+\frac{3}{2}\right)\upsilon_1+\frac{1}{4}z_2^4 \end{aligned} \tag{32}$$

Based on (32), the virtual control law α_1 and the adaptive laws $\dot{\hat{W}}_1, \dot{\hat{\iota}}_1$ are selected as

$$\alpha_1 = -k_1 z_1-\hat{W}_1\Xi_1-\frac{\hat{\iota}_1 z_1^3}{\sqrt{z_1^6+\upsilon_1^2}} \tag{33a}$$

$$\dot{\hat{W}}_1 = z_1^3\Xi_1-\upsilon_1\hat{W}_1 \tag{33b}$$

$$\dot{\hat{\iota}}_1 = \frac{z_1^6}{\sqrt{z_1^6+\upsilon_1^2}}-\upsilon_1\hat{\iota}_1 \tag{33c}$$

where k_1 is a positive constant.

Then, substituting (33) into (32) yields

$$LV_1 \le -k_1 z_1^4+\upsilon_1\tilde{W}_1\hat{W}_1+\upsilon_1\tilde{\iota}_1\hat{\iota}_1+\frac{1}{4}z_2^4+\left(W_1+\iota_1+\frac{3}{2}\right)\upsilon_1 \tag{34}$$

Step $i(2 \le i \le n-1)$: According to (17) and (18), we obtain the derivative of z_i as

$$dz_i = \left(x_{i+1}+f_i-\nabla\alpha_{i-1}\right)dt+\bar{h}_i^{\mathrm{T}}d\boldsymbol{\omega} \tag{35}$$

where $\nabla\alpha_{i-1} = \sum_{j=1}^{i-1}\frac{\partial\alpha_{i-1}}{\partial x_j}\left(x_{j+1}+f_j\right)+\sum_{j=1}^{i-1}\frac{\partial\alpha_{i-1}}{\hat{W}_j}\dot{\hat{W}}_j+\sum_{j=1}^{i-1}\frac{\partial\alpha_{i-1}}{\hat{\iota}_j}\dot{\hat{\iota}}_j+\sum_{j=0}^{i-1}\frac{\partial\alpha_{i-1}}{\partial y_d^{(j)}}y_d^{(j+1)}+\frac{1}{2}\sum_{j,k=1}^{i-1}\frac{\partial^2\alpha_{i-1}}{\partial x_j\partial x_k}h_j^{\mathrm{T}}h_k$ and $\bar{h}_i = h_i-\sum_{j=1}^{i-1}\frac{\partial\alpha_{i-1}}{\partial x_j}h_j$.

To achieve ATC, the following i-th Lyapunov function is chosen

$$V_i = V_{i-1}+\frac{1}{4}z_i^4+\frac{1}{2}\tilde{W}_i^2+\frac{1}{2}\tilde{\iota}_i^2 \tag{36}$$

where $\tilde{W}_i$ and $\tilde{\iota}_i$ are defined in (20).

By using Definition 1 on (35) and (36), we get

$$\begin{aligned} LV_i = & LV_{i-1}+z_i^3\left(\left(z_{i+1}+\alpha_i\right)+f_i-\nabla\alpha_{i-1}\right) \\ &+\frac{3}{2}z_i^2\mathrm{H}_i-\tilde{W}_i\dot{\hat{W}}_i-\tilde{\iota}_i\dot{\hat{\iota}}_i \end{aligned} \tag{37}$$

where $\mathrm{H}_i = \left\|\bar{h}_i\right\|^2$.

Then, with the help of Lemma 6 and Young's Inequality, the following two inequalities are obtained

$$z_i^3 z_{i+1} \le \frac{3}{4}z_i^4+\frac{1}{4}z_{i+1}^4 \tag{38}$$

$$\frac{3}{2}z_i^2\mathrm{H}_i \le \frac{3}{2}z_i^3\Phi_i+\frac{3}{2}\upsilon_i \tag{39}$$

By combining (38) and (39), (37) can be rewritten as

$$\begin{aligned} LV_i \le & LV_{i-1}+z_i^3\left(\alpha_i+\mathrm{T}_i+\frac{3}{2}\Phi_i\right) \\ &-\frac{1}{4}z_i^4+\frac{1}{4}z_{i+1}^4+\frac{3}{2}\upsilon_i-\tilde{W}_i\dot{\hat{W}}_i-\tilde{\iota}_i\dot{\hat{\iota}}_i \end{aligned} \tag{40}$$

where $\mathrm{T}_i = f_i-\nabla\alpha_{i-1}+z_i$.

Similarly, T_i is an unknown smooth non-linear function, so for $\forall\varepsilon_i > 0$, there exists an MTN that is used to approximate it as follows

$$\mathrm{T}_i = \boldsymbol{\varphi}_i^{\mathrm{T}}\mathrm{P}_{m_i}(Z_i)+\delta(Z_i), \left|\delta_i(Z_i)\right| \le \varepsilon_i \tag{41}$$

where $Z_i = [z_1, \ldots, z_i, y_d, \ldots, y_d^{(i)}, \hat{W}_1, \ldots, \hat{W}_{i-1}, \hat{\iota}_1, \ldots, \hat{\iota}_{i-1}]^{\mathrm{T}}$ and $\delta_i(Z_i)$ represent the input vector and the approximation error of MTN, respectively.

According to (19) and (41), and similar to the derivation of (30), we get

$$z_i^3\left(\mathrm{T}_i+\frac{3}{2}\Phi_i\right) \le W_i z_i^3\Xi_i+W_i\upsilon_i+\left|z_i^3\right|\iota_i \tag{42}$$

Then, using the Lemma 4, we can further get the following inequality

$$\left|z_i^3\right|\iota_i \le \frac{\iota_i z_i^6}{\sqrt{z_i^6+\upsilon_i^2}}+\iota_i\upsilon_i \tag{43}$$

By combining (42) and (43), the (40) can be expressed as

$$\begin{aligned} LV_i \le & LV_{i-1}+z_i^3\alpha_i+\hat{W}_i z_i^3\Xi_i+\frac{\hat{\iota}_i z_i^6}{\sqrt{z_i^6+\upsilon_i^2}} \\ &-\tilde{W}_i\left(\dot{\hat{W}}_i-z_i^3\Xi_i\right)-\tilde{\iota}_i\left(\dot{\hat{\iota}}_i-\frac{z_i^6}{\sqrt{z_i^6+\upsilon_i^2}}\right) \\ &+\left(W_i+\iota_i+\frac{3}{2}\right)\upsilon_i-\frac{1}{4}z_i^4+\frac{1}{4}z_{i+1}^4 \end{aligned} \tag{44}$$

Based on (44), the virtual control law α_i and the adaptive laws $\dot{\hat{W}}_i$, $\dot{\hat{\iota}}_i$ are selected as

$$\alpha_i = -k_i z_i-\hat{W}_i\Xi_i-\frac{\hat{\iota}_i z_i^3}{\sqrt{z_i^6+\upsilon_i^2}} \tag{45a}$$

10991239, 2025, 6, Downloaded from https://onlinelibrary.wiley.com/doi/10.1002/rnc.7799 by QINGDAO UNIVERSITY OF SCIENCE & TECH, Wiley Online Library on [04/03/2026]. See the Terms and Conditions (https://onlinelibrary.wiley.com/terms-and-conditions) on Wiley Online Library for rules of use; OA articles are governed by the applicable Creative Commons License

$$\dot{\hat{W}}_i = z_i^3 \Xi_i - \upsilon_i \hat{W}_i \tag{45b}$$

$$\dot{\hat{\imath}}_i = \frac{z_i^6}{\sqrt{z_i^6 + \upsilon_i^2}} - \upsilon_i \hat{\imath}_i \tag{45c}$$

where k_i is a positive constant.

Then, substituting (45) into (44) yields

$$\begin{aligned} LV_i \le & -\sum_{j=1}^{i} k_j z_j^4 + \sum_{j=1}^{i} \upsilon_j \tilde{W}_j \hat{W}_j + \sum_{j=1}^{i} \upsilon_j \tilde{\imath}_j \hat{\imath}_j \\ & + \sum_{j=1}^{i} \left(W_j + \imath_j + \frac{3}{2} \right) \upsilon_j + \frac{1}{4} z_{i+1}^4 \end{aligned} \tag{46}$$

Step n: According to (17) and (18), we obtain the derivative of z_n as

$$dz_n = \left(\left(\rho_1 \vartheta_s + \rho_2 \xi \right) + f_n - \nabla \alpha_{n-1} \right) dt + \overline{h}_n^{\mathrm{T}} d\boldsymbol{\omega} \tag{47}$$

where $\nabla \alpha_{n-1} = \sum_{j=1}^{n-1} \frac{\partial \alpha_{n-1}}{\partial x_j} \left(x_{j+1} + f_j \right) + \sum_{j=1}^{n-1} \frac{\partial \alpha_{n-1}}{\partial \hat{W}_j} \dot{\hat{W}}_j + \sum_{j=1}^{n-1} \frac{\partial \alpha_{n-1}}{\partial \hat{\imath}_j} \dot{\hat{\imath}}_j + \sum_{j=0}^{n-1} \frac{\partial \alpha_{n-1}}{\partial y_d^{(j)}} y_d^{(j+1)} + \frac{1}{2} \sum_{j,k=1}^{n-1} \frac{\partial^2 \alpha_{n-1}}{\partial x_j \partial x_k} h_j^{\mathrm{T}} h_k$ and $\overline{h}_n = h_n - \sum_{j=1}^{n-1} \frac{\partial \alpha_{n-1}}{\partial x_j} h_j$.

To achieve ATC, the following n-th Lyapunov function is chosen

$$V_n = V_{n-1} + \frac{1}{4} z_n^4 + \frac{1}{2} \tilde{W}_n^2 + \frac{1}{2} \tilde{\imath}_n^2 \tag{48}$$

where $\tilde{W}_n$ and $\tilde{\imath}_n$ are defined in (20).

By using Definition 1 on (47) and (48), we get

$$\begin{aligned} LV_n = & LV_{n-1} + \frac{3}{2} z_n^2 \mathrm{H}_n - \tilde{W}_n \dot{\hat{W}}_n - \tilde{\imath}_n \dot{\hat{\imath}}_n \\ & + z_n^3 \left(\left(\rho_1 \left(z_{n+1} + \alpha_n \right) + \rho_2 \xi \right) + f_n - \nabla \alpha_{n-1} \right) \end{aligned} \tag{49}$$

where $\mathrm{H}_n = \left\| \overline{h}_n \right\|^2$.

Since the direction ρ_1 of hysteresis is unknown, the control design is more complex. By introducing Nussbaum-type function $N(\eta) = \eta^2 \cos(\eta)$, a novel auxiliary part $\overline{\alpha}_n$ is ingeniously constructed for virtual control signal $\alpha_n = -N(\eta)\overline{\alpha}_n$ to solve this problem, and the value of η can be gotten through equation $\dot{\eta} = -\aleph z_n^3 \overline{\alpha}_n$. Thus, we have

$$\begin{aligned} z_n^3 \rho_1 \alpha_n &= -\left(\rho_1 N(\eta) + 1 \right) z_n^3 \overline{\alpha}_n + z_n^3 \overline{\alpha}_n \\ &= \frac{1}{\aleph} \left(\rho_1 N(\eta) + 1 \right) \dot{\eta} + z_n^3 \overline{\alpha}_n \end{aligned} \tag{50}$$

Then, according to Young's Inequality and Lemma 6, the following two inequalities are obtained

$$z_n^3 \rho_1 z_{n+1} \le \frac{3}{4} \rho_1^{\frac{4}{3}} z_n^4 + \frac{1}{4} z_{n+1}^4 \tag{51}$$

$$\frac{3}{2} z_n^2 \mathrm{H}_n \le \frac{3}{2} z_n^3 \Phi_n + \frac{3}{2} \upsilon_n \tag{52}$$

By combining (50–52), the (49) can be rewritten as

$$\begin{aligned} LV_n \le & LV_{n-1} + z_n^3 \left(\overline{\alpha}_n + \mathrm{T}_n + \frac{3}{2} \Phi_n \right) - \frac{1}{4} z_n^4 + \frac{1}{4} z_{n+1}^4 \\ & + \frac{3}{2} \upsilon_n + \frac{1}{\aleph} \left(\rho_1 N(\eta) + 1 \right) \dot{\eta} - \tilde{W}_n \dot{\hat{W}}_n - \tilde{\imath}_n \dot{\hat{\imath}}_n \end{aligned} \tag{53}$$

where $\mathrm{T}_n = f_n - \nabla \alpha_{n-1} + \frac{3}{4} \rho_1^{\frac{4}{3}} z_n + \rho_2 \xi + \frac{1}{4} z_n$.

Similarly, T_n is an unknown smooth non-linear function, so for $\forall \varepsilon_n > 0$, there exists an MTN that is used to approximate it as follows

$$\mathrm{T}_n = \boldsymbol{\varphi}_n^{\mathrm{T}} \mathrm{P}_{m_n} \left(Z_n \right) + \delta \left(Z_n \right), \left| \delta_n \left(Z_n \right) \right| \le \varepsilon_n \tag{54}$$

where $Z_n = [z_1, \ldots, z_n, y_d, \ldots, y_d^{(n)}, \hat{W}_1, \ldots, \hat{W}_{n-1}, \hat{\imath}_1, \ldots, \hat{\imath}_{n-1}]^{\mathrm{T}}$ and $\delta_n \left(Z_n \right)$ represent the input vector and the approximation error of MTN, respectively.

According to (19) and (54), and similar to the derivation of (30), we get

$$z_n^3 \left(\mathrm{T}_n + \frac{3}{2} \Phi_n \right) \le W_n z_n^3 \Xi_n + W_n \upsilon_n + \left| z_n^3 \right| \imath_n \tag{55}$$

Then, using the Lemma 4, we can further get the following inequality

$$\left| z_n^3 \right| \imath_n \le \frac{\imath_n z_n^6}{\sqrt{z_n^6 + \upsilon_n^2}} + \imath_n \upsilon_n \tag{56}$$

By combining (55) and (56), (53) can be expressed as

$$\begin{aligned} LV_n \le & LV_{n-1} + z_n^3 \overline{\alpha}_n + \hat{W}_n z_n^3 \Xi_n + \frac{\hat{\imath}_n z_n^6}{\sqrt{z_n^6 + \upsilon_n^2}} \\ & - \tilde{W}_n \left(\dot{\hat{W}}_n - z_n^3 \Xi_n \right) - \tilde{\imath}_n \left(\dot{\hat{\imath}}_n - \frac{z_n^6}{\sqrt{z_n^6 + \upsilon_n^2}} \right) \\ & + \left(W_n + \imath_n + \frac{3}{2} \right) \upsilon_n + \frac{1}{\aleph} \left(\rho_1 N(\eta) + 1 \right) \dot{\eta} - \frac{1}{4} z_n^4 + \frac{1}{4} z_{n+1}^4 \end{aligned} \tag{57}$$

Based on (57), the auxiliary part $\overline{\alpha}_n$, the virtual control law α_n and the adaptive laws $\dot{\hat{W}}_n$, $\dot{\hat{\imath}}_n$ are selected as

$$\overline{\alpha}_n = -k_n z_n - \hat{W}_n \Xi_n - \frac{\hat{\imath}_n z_n^3}{\sqrt{z_n^6 + \upsilon_n^2}} \tag{58a}$$

$$\alpha_n = -N(\eta) \overline{\alpha}_n \tag{58b}$$

$$\dot{\hat{W}}_n = z_n^3 \Xi_n - \upsilon_n \hat{W}_n \tag{58c}$$

$$\dot{\hat{\imath}}_n = \frac{z_n^6}{\sqrt{z_n^6 + \upsilon_n^2}} - \upsilon_n \hat{\imath}_n \tag{58d}$$

where k_n is a positive constant.

10991239, 2025, 6, Downloaded from https://onlinelibrary.wiley.com/doi/10.1002/rnc.7799 by QINGDAO UNIVERSITY OF SCIENCE & TECH, Wiley Online Library on [04/03/2026]. See the Terms and Conditions (https://onlinelibrary.wiley.com/terms-and-conditions) on Wiley Online Library for rules of use; OA articles are governed by the applicable Creative Commons License

Then, substituting (58) into (57) yields

$$LV_n \le -\sum_{j=1}^{n} k_j z_j^4 + \sum_{j=1}^{n} \upsilon_j \tilde{W}_j \hat{W}_j + \sum_{j=1}^{n} \upsilon_j \tilde{\imath}_j \hat{\imath}_j + \sum_{j=1}^{n} \left(W_j + \imath_j + \frac{3}{2} \right) \upsilon_j + \frac{1}{\aleph} \left(\rho_1 N(\eta) + 1 \right) \dot{\eta} + \frac{1}{4} z_{n+1}^4 \tag{59}$$

Step $n+1$: According to (17) and (18), the derivative of z_{n+1} can be obtained as

$$dz_{n+1} = \left(b\left(\vartheta - \vartheta_s \right) + f_{n+1} - \nabla \alpha_n \right) dt + \overline{h}_{n+1}^{\mathrm{T}} d\boldsymbol{\omega} \tag{60}$$

where $\nabla \alpha_n = \sum_{j=1}^{n-1} \frac{\partial \alpha_n}{\partial x_j} \left(x_{j+1} + f_j \right) + \frac{\partial \alpha_n}{\partial x_n} \left(\rho_1 \vartheta_s + \rho_2 \xi + f_n \right) + \sum_{j=1}^{n} \frac{\partial \alpha_n}{\partial \hat{W}_j} \dot{\hat{W}}_j + \sum_{j=1}^{n} \frac{\partial \alpha_n}{\partial \hat{\imath}_j} \dot{\hat{\imath}}_j + \sum_{j=0}^{n} \frac{\partial \alpha_n}{\partial y_d^{(j)}} y_d^{(j+1)} + \frac{1}{2} \sum_{j,k=1}^{n} \frac{\partial^2 \alpha_n}{\partial x_j \partial x_k} h_j^{\mathrm{T}} h_k$ and $\overline{h}_{n+1} = -\sum_{j=1}^{n} \frac{\partial \alpha_n}{\partial x_j} h_j$.

To achieve ATC, the following $n+1$-th Lyapunov function is chosen

$$V_{n+1} = V_n + \frac{1}{4} z_{n+1}^4 + \frac{1}{2} \tilde{W}_{n+1}^2 + \frac{1}{2} \tilde{\imath}_{n+1}^2 \tag{61}$$

where $\tilde{W}_{n+1}$ and $\tilde{\imath}_{n+1}$ are defined in (20).

TABLE 1 | Parameters of Example 1.

Parameter	Value	Parameter	Value	Parameter	Value
k_1	20	γ	2	$\hbar$	10
k_2	4	β	1	ς	0.1
k_3	4	A	1	υ_1	$5e^{-0.1t}$
b	10	n	2	υ_2	$2e^{-0.5t}$
$\aleph$	10	m	2	υ_3	$20e^{-0.01t}$
ρ_1	1	m_1	0.5		
ρ_2	1	$\overline{m}$	3		

By using Definition 1 on (60) and (61), we get

$$LV_{n+1} = LV_n + z_{n+1}^3 \left(b\left(\vartheta - \vartheta_s \right) + f_{n+1} - \nabla \alpha_n \right) + \frac{3}{2} z_{n+1}^2 \mathrm{H}_{n+1} - \tilde{W}_{n+1} \dot{\hat{W}}_{n+1} - \tilde{\imath}_{n+1} \dot{\hat{\imath}}_{n+1} \tag{62}$$

where $\mathrm{H}_{n+1} = \left\| \overline{h}_{n+1} \right\|^2$.

Then, by using the Lemma 6, the following inequality is obtained

$$\frac{3}{2} z_{n+1}^2 \mathrm{H}_{n+1} \le \frac{3}{2} z_{n+1}^3 \Phi_{n+1} + \frac{3}{2} \upsilon_{n+1} \tag{63}$$

Substituting (63) into (62) yields

$$LV_{n+1} = LV_n + z_{n+1}^3 \left(b\vartheta + \mathrm{T}_{n+1} + \frac{3}{2} \Phi_{n+1} \right) - \frac{1}{4} z_{n+1}^4 + \frac{3}{2} \upsilon_{n+1} - \tilde{W}_{n+1} \dot{\hat{W}}_{n+1} - \tilde{\imath}_{n+1} \dot{\hat{\imath}}_{n+1} \tag{64}$$

where $\mathrm{T}_{n+1} = f_{n+1} - \nabla \alpha_n - b\vartheta_s + \frac{1}{4} z_{n+1}$.

Similarly, T_{n+1} is an unknown smooth non-linear function, so for $\forall \varepsilon_{n+1} > 0$, there exists an MTN that is used to approximate it as follows

$$\mathrm{T}_{n+1} = \boldsymbol{\varphi}_{n+1}^{\mathrm{T}} \mathrm{P}_{m_{n+1}} \left(Z_{n+1} \right) + \delta \left(Z_{n+1} \right), \left| \delta_{n+1} \left(Z_{n+1} \right) \right| \le \varepsilon_{n+1} \tag{65}$$

where $Z_{n+1} = [z_1, \ldots, z_{n+1}, y_d, \ldots, y_d^{(n+1)}, \hat{W}_1, \ldots, \hat{W}_n, \hat{\imath}_1, \ldots, \hat{\imath}_n]^{\mathrm{T}}$ and $\delta_{n+1} \left(Z_{n+1} \right)$ represent the input vector and the approximation error of MTN, respectively.

According to (19) and (65), and similar to the derivation of (30), we get

$$z_{n+1}^3 \left(\mathrm{T}_{n+1} + \frac{3}{2} \Phi_{n+1} \right) \le W_{n+1} z_{n+1}^3 \Xi_{n+1} + W_{n+1} \upsilon_{n+1} + \left| z_{n+1}^3 \right| \imath_{n+1} \tag{66}$$

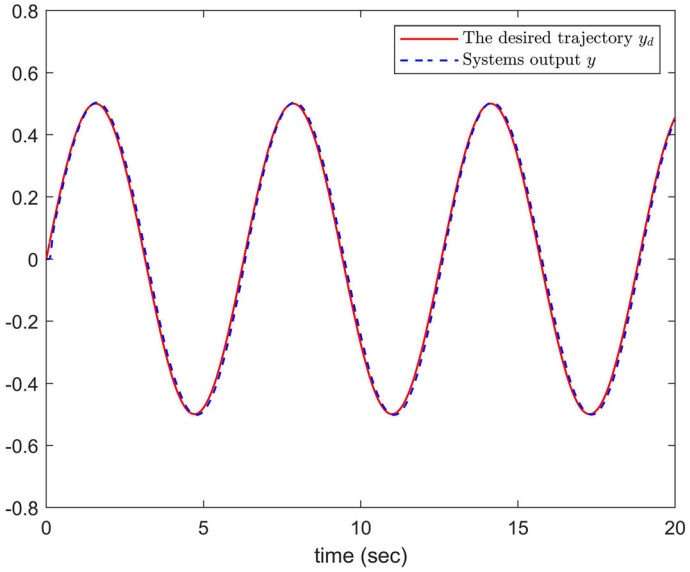

FIGURE 3 | The trajectories of y_d and y of Example 1.

10991239, 2025, 6, Downloaded from https://onlinelibrary.wiley.com/doi/10.1002/rnc.7799 by QINGDAO UNIVERSITY OF SCIENCE & TECH, Wiley Online Library on [04/03/2026]. See the Terms and Conditions (https://onlinelibrary.wiley.com/terms-and-conditions) on Wiley Online Library for rules of use; OA articles are governed by the applicable Creative Commons License

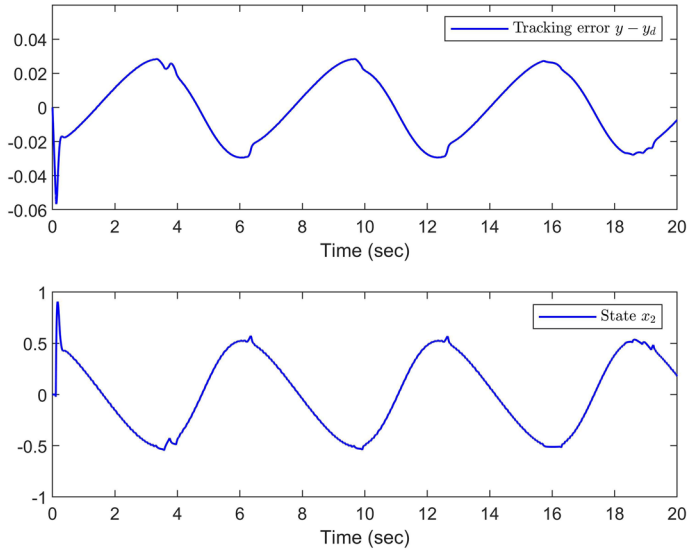

FIGURE 4 | The trajectories of tracking error $y - y_d$ and state x_2 of Example 1.

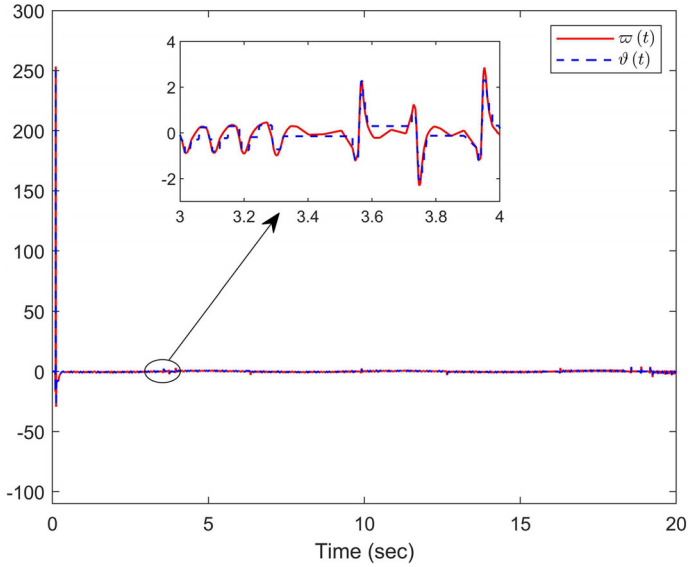

FIGURE 5 | The trajectories of controller $\varpi(t)$ and control signal $\vartheta(t)$ of Example 1.

Then, using the Lemma 4, we can further get the following inequality

$$\left|z_{n+1}^3\right|\iota_{n+1} \leq \frac{\iota_{n+1} z_{n+1}^6}{\sqrt{z_{n+1}^6 + \upsilon_{n+1}^2}} + \iota_{n+1}\upsilon_{n+1} \tag{67}$$

By combining (66) and (67), the (64) can be expressed as

$$\begin{aligned} LV_{n+1} \leq\ & LV_n + z_{n+1}^3 b\vartheta + \hat{W}_{n+1} z_{n+1}^3 \Xi_{n+1} + \frac{\hat{\iota}_{n+1} z_{n+1}^6}{\sqrt{z_{n+1}^6 + \upsilon_{n+1}^2}} \\ & - \tilde{W}_{n+1}\left(\dot{\hat{W}}_{n+1} - z_{n+1}^3 \Xi_{n+1}\right) \\ & - \tilde{\iota}_{n+1}\left(\dot{\hat{\iota}}_{n+1} - \frac{z_{n+1}^6}{\sqrt{z_{n+1}^6 + \upsilon_{n+1}^2}}\right) \\ & + \left(W_{n+1} + \iota_{n+1} + \frac{3}{2}\right)\upsilon_{n+1} - \frac{1}{4} z_{n+1}^4 \end{aligned} \tag{68}$$

Based on (68), the event-triggered controller ϖ, the virtual control law α_{n+1} and the adaptive laws $\dot{\hat{W}}_{n+1}, \dot{\hat{\iota}}_{n+1}$ are selected as

$$\varpi(t) = \alpha_{n+1} - \overline{m}\tanh\left(\frac{z_{n+1}^3 \overline{m}}{\upsilon_{n+1}}\right) \tag{69a}$$

$$\alpha_{n+1} = \frac{1}{b}\left(-k_{n+1} z_{n+1} - \hat{W}_{n+1}\Xi_{n+1} - \frac{\hat{\iota}_{n+1} z_{n+1}^3}{\sqrt{z_{n+1}^6 + \upsilon_{n+1}^2}}\right) \tag{69b}$$

$$\dot{\hat{W}}_{n+1} = z_{n+1}^3 \Xi_{n+1} - \upsilon_{n+1}\hat{W}_{n+1} \tag{69c}$$

$$\dot{\hat{\iota}}_{n+1} = \frac{z_{n+1}^6}{\sqrt{z_{n+1}^6 + \upsilon_{n+1}^2}} - \upsilon_{n+1}\hat{\iota}_{n+1} \tag{69d}$$

10991239, 2025, 6, Downloaded from https://onlinelibrary.wiley.com/doi/10.1002/rnc.7799 by QINGDAO UNIVERSITY OF SCIENCE & TECH, Wiley Online Library on [04/03/2026]. See the Terms and Conditions (https://onlinelibrary.wiley.com/terms-and-conditions) on Wiley Online Library for rules of use; OA articles are governed by the applicable Creative Commons License

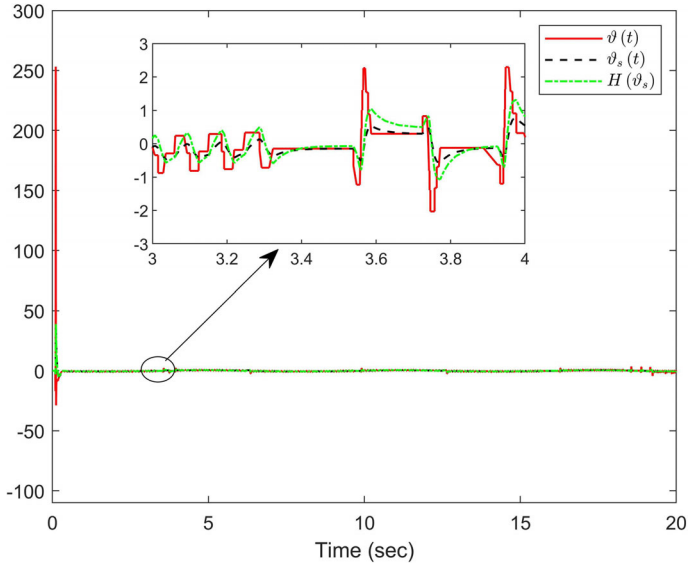

FIGURE 6 | The trajectories of filter output signal $\vartheta_s(t)$ and hysteresis output signal $H(\vartheta_s)$ of Example 1.

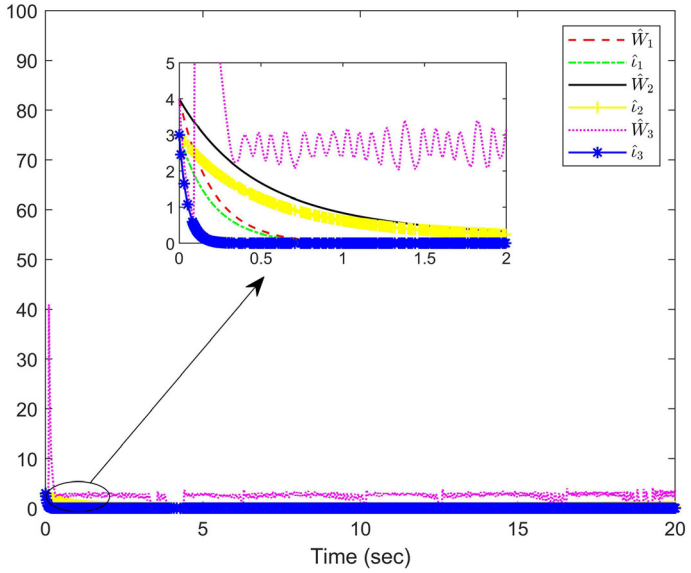

FIGURE 7 | The trajectories of adaptive parameters $\hat{W}_i, i = 1, 2, 3$ and $\hat{\iota}_i, i = 1, 2, 3$ of Example 1.

where k_{n+1} and $\overline{m} \geq e_1$ are positive constants.

Remark 5. In time interval $t \in [t_k, t_{k+1})$, from (7) and (8), we can get $\varpi(t) = \vartheta(t) + \lambda(t)e_1$, where $\lambda(t)$ is time-varying parameter satisfying $|\lambda(t)| < 1$. Thus, we have $\vartheta(t) = \varpi(t) - \lambda(t)e_1$.

Then, substituting (69) into (68), and using Lemma 5 simultaneously yields

$$LV_{n+1} \leq -\sum_{j=1}^{n+1} k_j z_j^4 - b\left|z_{n+1}^3 \overline{m}\right| - b\lambda(t) z_{n+1}^3 e_1 + \sum_{j=1}^{n+1} \upsilon_j \tilde{W}_j \hat{W}_j + \sum_{j=1}^{n+1} \upsilon_j \tilde{\iota}_j \hat{\iota}_j + \sum_{j=1}^{n} \left(W_j + \iota_j + \frac{3}{2}\right)\upsilon_j + \left(W_{n+1} + \iota_{n+1} + \frac{3}{2} + 0.2785b\right)\upsilon_{n+1} + \frac{1}{\aleph}\left(\rho_1 N(\eta) + 1\right)\dot{\eta} \tag{70}$$

Furthermore, the following inequalities hold

$$\tilde{W}_j \hat{W}_j = \tilde{W}_j\left(W_j - \tilde{W}_j\right) = -\tilde{W}_j^2 + \tilde{W}_j W_j \leq -\frac{1}{2}\tilde{W}_j^2 + \frac{1}{2}W_j^2 \tag{71}$$

$$\tilde{\iota}_j \hat{\iota}_j = \tilde{\iota}_j\left(\iota_j - \tilde{\iota}_j\right) = -\tilde{\iota}_j^2 + \tilde{\iota}_j \iota_j \leq -\frac{1}{2}\tilde{\iota}_j^2 + \frac{1}{2}\iota_j^2 \tag{72}$$

By combing (71) and (72), the (70) can be transformed into the following inequality

10991239, 2025, 6, Downloaded from https://onlinelibrary.wiley.com/doi/10.1002/rnc.7799 by QINGDAO UNIVERSITY OF SCIENCE & TECH, Wiley Online Library on [04/03/2026]. See the Terms and Conditions (https://onlinelibrary.wiley.com/terms-and-conditions) on Wiley Online Library for rules of use; OA articles are governed by the applicable Creative Commons License

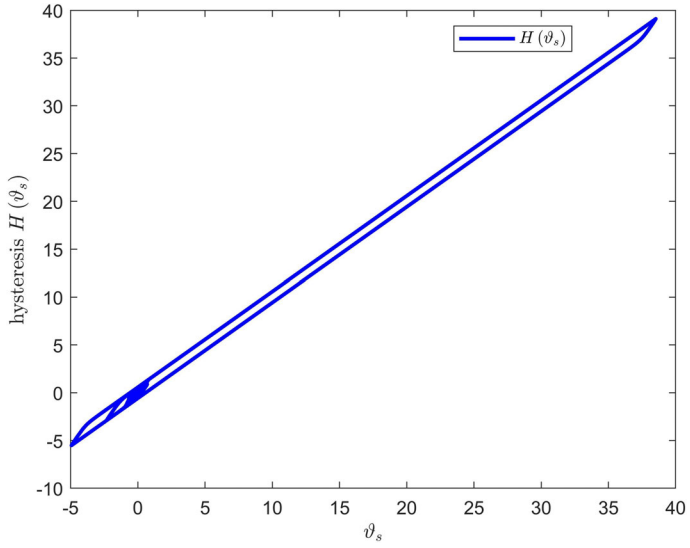

FIGURE 8 | The trajectories of hysteresis of Example 1.

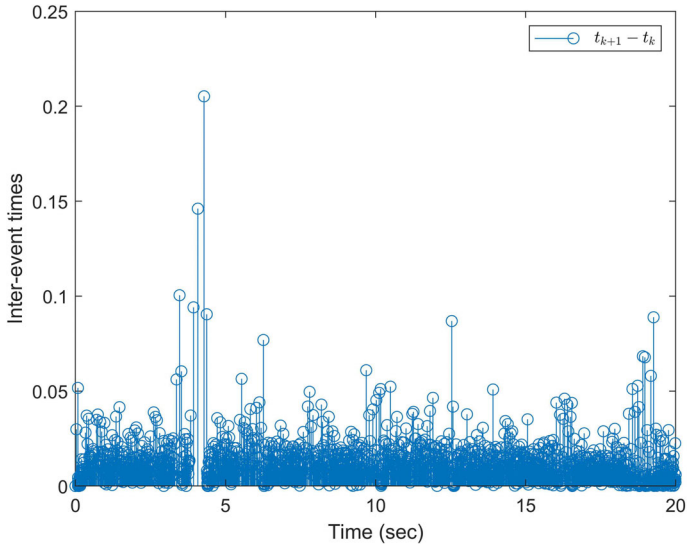

FIGURE 9 | The triggering moments and interevent intervals of Example 1.

TABLE 2 | Parameters of Example 2.

Parameter	Value	Parameter	Value	Parameter	Value
M	1	$\aleph$	20	m_1	1
B	1	ρ_1	3	$\overline{m}$	5.5
m_2	1	ρ_2	2	$\hbar$	10
l	1	A	1	ς	0.05
k_1	25	γ	2	υ_1	$10e^{-0.01t}$
k_2	3	β	1	υ_2	$20e^{-0.01t}$
k_3	3	n	2	υ_3	$30e^{-0.01t}$
b	2.5	m	2		

$$LV_{n+1} \le -\sum_{j=1}^{n+1} k_j z_j^4 - \sum_{j=1}^{n+1}\left(\frac{\tilde{W}_j^2 + \tilde{\imath}_j^2}{2}\right)\upsilon_j + \sum_{j=1}^{n+1} o_j \upsilon_j + \frac{1}{\aleph}\left(\rho_1 N(\eta)+1\right)\dot{\eta} \tag{73}$$

where $o_j = \frac{W_j^2+\imath_j^2}{2} + W_j + \imath_j + \frac{3}{2}, j = 1, \ldots, n$, $o_{n+1} = \frac{W_{n+1}^2+\imath_{n+1}^2}{2} + W_{n+1} + \imath_{n+1} + \frac{3}{2} + 0.2785b$.

Remark 6. In this paper, the application of the bounded estimation method and defining variable $\imath_i$ makes the existence of stochastic disturbances to be subtly eliminated. Moreover, by introducing function υ_i and constructing smooth functions Ξ_i, Φ_i, the ATC of system (17) can be achieved.

10991239, 2025, 6, Downloaded from https://onlinelibrary.wiley.com/doi/10.1002/rnc.7799 by QINGDAO UNIVERSITY OF SCIENCE & TECH, Wiley Online Library on [04/03/2026]. See the Terms and Conditions (https://onlinelibrary.wiley.com/terms-and-conditions) on Wiley Online Library for rules of use; OA articles are governed by the applicable Creative Commons License

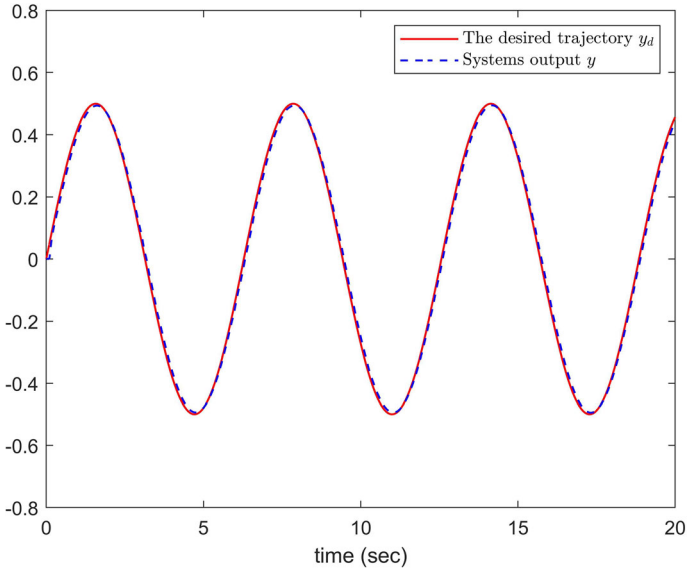

FIGURE 10 | The trajectories of y_d and y of Example 2.

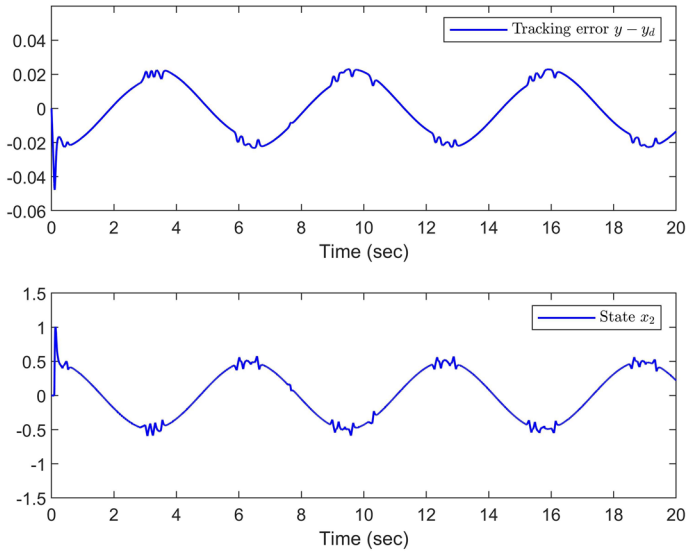

FIGURE 11 | The trajectories of tracking error $y - y_d$ and state x_2 of Example 2.

Remark 7. It is worth noting that whenever the controller is triggered under huge signal amplitude, the system will inevitably be subjected to strong signal impulses, so the FTM is adapted to provide a bounded measurement error to maintain the regular operation of the system components, thus indirectly optimizing the asymptotic tracking performance of the system. Otherwise, when the signal amplitude is small, the RTM is used to obtain more precise control performance. Therefore, the system's asymptotic tracking performance and control performance are intelligently balanced, further improving the asymptotic tracking performance of the controller. In addition to that, since the simple structure of MTN was elaborated in [11, 13, 48], the event-triggered adaptive MTN asymptotic tracking controller is designed in this paper with lower energy consumption.

3.2 | Stability Analysis

Theorem 1. *Considering the stochastic non-linear system (1) subject to unknown hysteresis and limited network resources, the proposed event-triggered controller (69a), the virtual control laws (33a), (45a), (58b), (69b) and the adaptive laws (33b), (33c), (45b), (45c), (58c), (58d), (69c), (69d). For any bounded initial condition, we can conclude*

1. *all signals of the closed-loop system are bounded in probability on* $[0, +\infty)$;
2. *the system output with zero tracking error can be achieved*
3. *Zeno phenomenon is excluded.*

10991239, 2025, 6, Downloaded from https://onlinelibrary.wiley.com/doi/10.1002/rnc.7799 by QINGDAO UNIVERSITY OF SCIENCE & TECH, Wiley Online Library on [04/03/2026]. See the Terms and Conditions (https://onlinelibrary.wiley.com/terms-and-conditions) on Wiley Online Library for rules of use; OA articles are governed by the applicable Creative Commons License

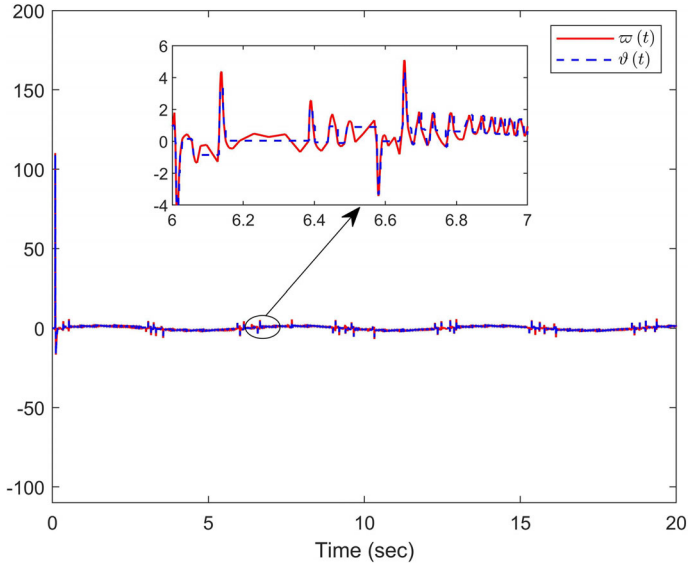

FIGURE 12 | The trajectories of controller $\varpi(t)$ and control signal $\vartheta(t)$ of Example 2.

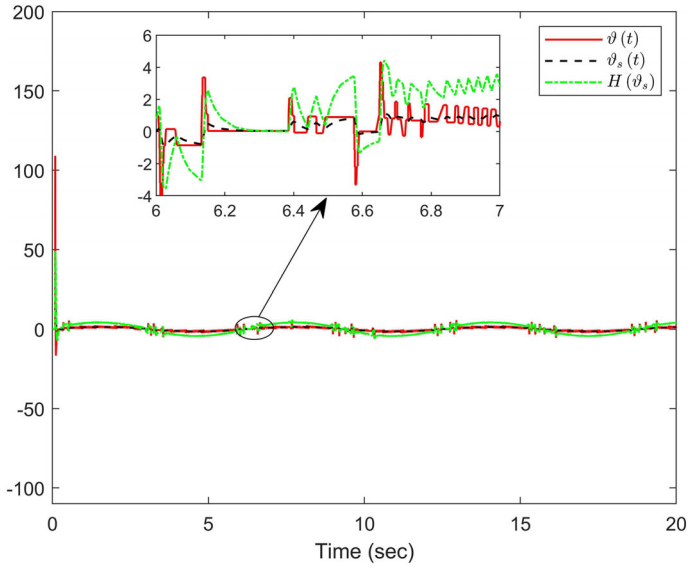

FIGURE 13 | The trajectories of filter output signal $\vartheta_s(t)$ and hysteresis output signal $H(\vartheta_s)$ of Example 2.

Proof. Since υ_i is a positive bounded and continuous function, there exist positive constants l_i and q such that $l_i \le \upsilon_i$ and $\sum_{j=1}^{n+1} o_j \upsilon_j \le q$. Next, let $p = \min\{4k_j, l_j, j = 1, 2, \ldots n+1\}$, the (73) can be rewritten as

$$LV_{n+1} \le -pV_{n+1} + \frac{1}{\aleph}\left(\rho_1 N(\eta) + 1\right)\dot{\eta} + q \tag{74}$$

Obviously, it can be obtained by using the $Itô$ formula

$$d\left(e^{pt}V_{n+1}\right) = e^{pt}\left(pV_{n+1} + LV_{n+1}\right)dt + e^{pt}\Lambda d\boldsymbol{\omega}(t) \tag{75}$$

where $\Lambda = \frac{\partial V_{n+1}}{\partial z_1}h_1^{\mathrm{T}} + \sum_{i=2}^{n}\frac{\partial V_{n+1}}{\partial z_i}\left(h_i - \sum_{j=1}^{i-1}\frac{\partial \alpha_{i-1}}{\partial x_j}h_j\right)^{\mathrm{T}} + \frac{\partial V_{n+1}}{\partial z_{n+1}}\left(-\sum_{j=1}^{n}\frac{\partial \alpha_n}{\partial x_j}h_j\right)^{\mathrm{T}}$.

Integrating (75) over 0 to t yields

$$\begin{aligned} V_{n+1}(t) \le\ & e^{-pt}V_{n+1}(0) + \frac{q}{p}\left(1 - e^{-pt}\right) \\ & + e^{-pt}\int_0^t \frac{1}{\aleph}\left(\rho_1 N(\eta) + 1\right)\dot{\eta}e^{p\sigma}d\sigma \\ & + e^{-pt}\int_0^t e^{p\sigma}\Lambda d\boldsymbol{\omega}(\sigma) \end{aligned} \tag{76}$$

According to (76) and Lemma 2, we can infer that $V_{n+1}(t)$ is bounded in probability on $[0, t_f)$. Therefore, z_i, $\tilde{W}_i$ and $\tilde{\imath}_i$ are also bounded in probability on $[0, t_f)$.

Since W_i and ι_i are constants, we can further prove that $\hat{W}_i$ and $\hat{\imath}_i$ are bounded in probability on $[0, t_f)$. And α_i is composed of

10991239, 2025, 6, Downloaded from https://onlinelibrary.wiley.com/doi/10.1002/rnc.7799 by QINGDAO UNIVERSITY OF SCIENCE & TECH, Wiley Online Library on [04/03/2026]. See the Terms and Conditions (https://onlinelibrary.wiley.com/terms-and-conditions) on Wiley Online Library for rules of use; OA articles are governed by the applicable Creative Commons License

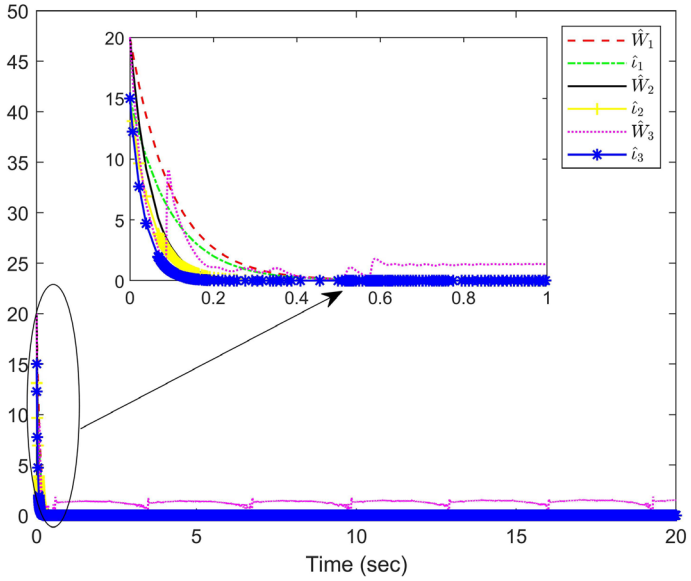

FIGURE 14 | The trajectories of adaptive parameters $\hat{W}_i, i = 1, 2, 3$ and $\hat{\imath}_i, i = 1, 2, 3$ of Example 2.

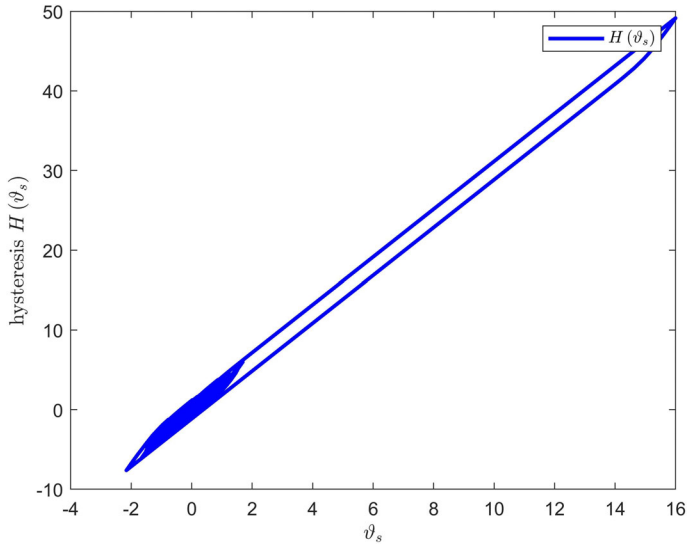

FIGURE 15 | The trajectories of hysteresis of Example 2.

bounded signals z_i, $\hat{W}_i$, $\hat{\imath}_i$ and bounded function υ_i, so it is also bounded in probability on $[0, t_f)$. In view of $z_i = x_i - \alpha_{i-1}$, we can get that x_i is bounded in probability on $[0, t_f)$. Moreover, we can get that the controller $\varpi(t)$, actuator input $\vartheta_s(t)$ and system input $H(\vartheta_s)$ are also bounded in probability on $[0, t_f)$. Because the solution of the closed-loop system is bounded, according to Lemma 2, we have $t_f \to \infty$. Thus, all signals of the closed-loop system are bounded in probability on $[0, +\infty)$.

Similar to the proof of Theorem 1 in [49], we can further get that the system output with zero tracking error and there is no Zeno phenomenon.

In summary, the correctness of Theorem 1 is proved. □

Remark 8. $\upsilon_i(t)$ is introduced to ensure asymptotic tracking effect, while k_i is added to ensure the better tracking performance. In theory, we can decrease $\upsilon_i(t)$ and increase k_i arbitrarily. However, as indicated by Equations (33a), (45a), (58a), and (69b), decreasing $\upsilon_i(t)$ or increasing k_i can lead to an increase in the amplitude of control signals. Therefore, a trade-off between tracking performance and control effort is necessary to achieve optimal control performance.

4 | Simulation Results

In this section, three simulation examples will be given to prove the effectiveness and superiority of the proposed control scheme.

Example 1. (Numerical example). Considering the following numerical example of a second-order stochastic

10991239, 2025, 6, Downloaded from https://onlinelibrary.wiley.com/doi/10.1002/rnc.7799 by QINGDAO UNIVERSITY OF SCIENCE & TECH, Wiley Online Library on [04/03/2026]. See the Terms and Conditions (https://onlinelibrary.wiley.com/terms-and-conditions) on Wiley Online Library for rules of use; OA articles are governed by the applicable Creative Commons License

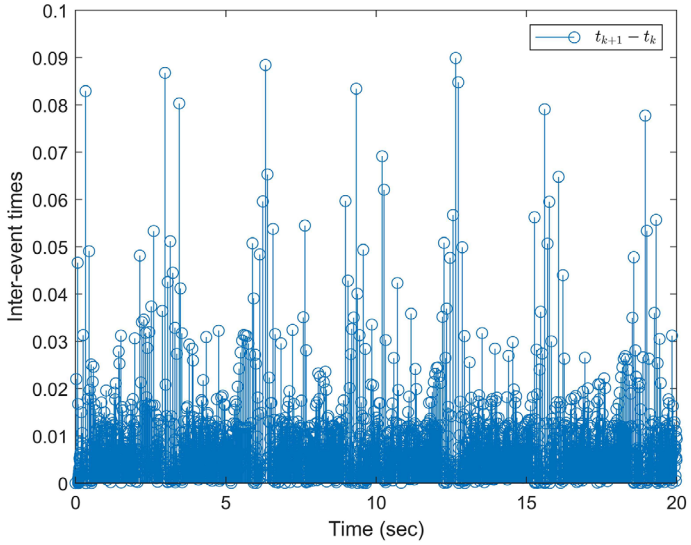

FIGURE 16 | The triggering moments and interevent intervals of Example 2.

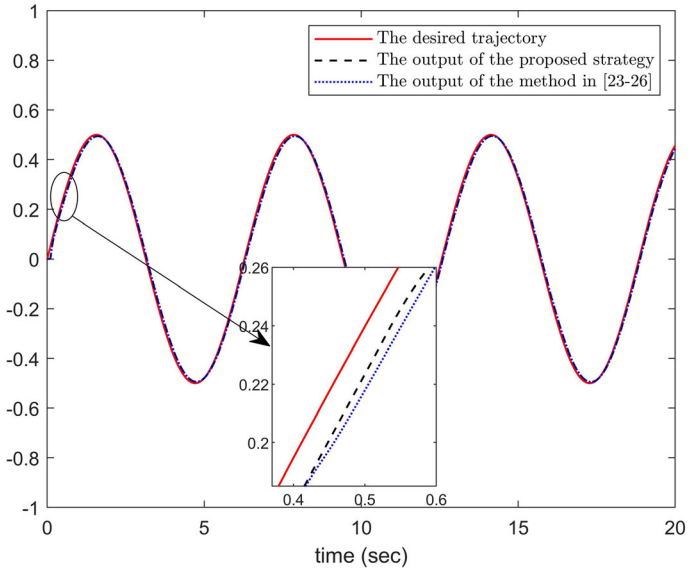

FIGURE 17 | The tracking trajectories of system (79) under two mechanisms.

non-linear system with unknown hysteresis.

$$\begin{cases} dx_1 = \left(x_2 + 0.5x_1x_2\right)dt \\ dx_2 = \left(H(\vartheta) + 0.3x_1^2\right)dt + 0.4\sin\left(x_1^2\right)d\boldsymbol{\omega} \\ y = x_1 \end{cases} \tag{77}$$

By introducing the first-order filter, the system (77) can be rewritten as

$$\begin{cases} dx_1 = \left(x_2 + 0.5x_1x_2\right)dt \\ dx_2 = \left(H\left(\vartheta_s\right) + 0.3x_1^2\right)dt + 0.4\sin\left(x_1^2\right)d\boldsymbol{\omega} \\ H\left(\vartheta_s\right) = \rho_1\vartheta_s + \rho_2\xi \\ d\vartheta_s = \left(b\left(\vartheta - \vartheta_s\right)\right)dt \\ y = x_1 \end{cases} \tag{78}$$

For system (78), select initial values as $[x_1(0), x_2(0), \vartheta_s(0)]^{\mathrm{T}} = [0, 0, 0]^{\mathrm{T}}$, $[W_1(0), W_2(0), W_3(0)]^{\mathrm{T}} = [4, 4, 4]^{\mathrm{T}}$, $[\iota_1(0), \iota_2(0), \iota_3(0)]^{\mathrm{T}} = [3, 3, 3]^{\mathrm{T}}$, and reference signal $y_d = 0.5\sin(t)$. Besides, the value of other relevant parameters is given in Table 1.

Figures 3–9 show the simulation results of system (78). Figure 3 displays the trajectories of the reference signal y_d and output signal y. Figure 4 depicts the trajectories of the state x_2 and tracking error $y - y_d$. Figure 5 illustrates the controller $\varpi(t)$ and control signal $\vartheta(t)$ generated by the ETM, which indicates that when $\vartheta(t)$ is too large, the FTM adopted in this paper will better protect the asymptotic tracking performance of the system; otherwise, when $\vartheta(t)$ is small, intelligently switch to RTM to obtain more precise control. Figure 6 shows the trajectories of filter output signal $\vartheta_s(t)$ and hysteresis output signal $H\left(\vartheta_s\right)$, which are smooth and differentiable signals. Figures 7 and 8 show the adaptive parameters $\hat{W}_i, i = 1, 2, 3$, $\hat{\iota}_i, i = 1, 2, 3$ and actuator hysteresis $H\left(\vartheta_s\right)$,

10991239, 2025, 6, Downloaded from https://onlinelibrary.wiley.com/doi/10.1002/rnc.7799 by QINGDAO UNIVERSITY OF SCIENCE & TECH, Wiley Online Library on [04/03/2026]. See the Terms and Conditions (https://onlinelibrary.wiley.com/terms-and-conditions) on Wiley Online Library for rules of use; OA articles are governed by the applicable Creative Commons License

respectively. All the triggering moments and interevent intervals are given in Figure 8. From Figures 3–9, we can conclude that the control strategy proposed in this paper is effective.

Example 2. (Practical example). A practical example of a second-order single-link manipulator is considered. According to [50] and introducing the first-order filter, its stochastic non-linear system model is reformulated as

$$\begin{cases} dx_1 = x_2 dt \\ dx_2 = \left(\frac{1}{M}H(\vartheta_s) - \frac{B}{M}x_2 - \frac{m_2 g l}{M}\sin(x_1)\right)dt + \frac{G(x_1^2)}{M}d\omega \\ H(\vartheta_s) = \rho_1 \vartheta_s + \rho_2 \xi \\ d\vartheta_s = \left(b(\vartheta - \vartheta_s)\right)dt \\ y = x_1 \end{cases} \tag{79}$$

where $G(x_1^2) = 0.1\sin(x_1^2)$.

In simulation, select initial values as $[x_1(0), x_2(0), \vartheta_s(0)]^{\mathrm{T}} = [0,0,0]^{\mathrm{T}}$, $[W_1(0), W_2(0), W_3(0)]^{\mathrm{T}} = [20,20,20]^{\mathrm{T}}$, $[\iota_1(0), \iota_2(0), \iota_3(0)]^{\mathrm{T}} = [15,15,15]^{\mathrm{T}}$, and reference signal $y_d = 0.5\sin(t)$. Besides, the value of other relevant parameters is given in Table 2.

Figures 10–16 show that the proposed control objectives can be implemented for a practical single-link robot system. The above simulation results further verify the effectiveness and practical application value of the proposed control strategy.

Example 3. To verify the advantages of the proposed STM-based ETC strategy in achieving asymptotic tracking, an experiment was conducted on system (79), comparing its performance with that of the RTM-based ETC strategy outlined in [25–28].

From Figure 17, it is evident that $\vartheta(t)$ exhibits relatively large amplitude fluctuations in the 0.4–0.6 s range. Consequently, through the theoretical analysis presented in Remark 7 and the locally magnified simulation results in Figure 17, it is demonstrated that when $\vartheta(t)$ reaches a higher value, the novel STM proposed in this paper indirectly enhances the system's asymptotic tracking performance by maintaining the regular operation of system components. Furthermore, the local enlarged image of the tracking trajectory in Figure 17 shows that the STM enhances the robustness of the system against stochastic disturbances and internal uncertainties, which further highlights the superiority of the control strategy proposed in this paper.

5 | Conclusion

In this paper, an STM-based event-triggered adaptive ATC scheme is proposed. By using the bounded estimation method and Nussbaum function, the proposed controller with lower energy consumption not only effectively compensates for stochastic disturbances and unknown hysteresis, but also optimizes the ATC performance of the system. Furthermore, a first-order filter is creatively used to avoid the contradiction between discrete signals generated by ETM and rate-dependent characteristics of actuator hysteresis, and an improved backstepping technique is applied to deal with additional states. The simulation examples show the effectiveness and superiority of the proposed control scheme. Future research will focus on the control of multi-agent systems, designing low-complexity controllers [51], while also studying the issue of fixed-time convergence. The research methods will be applied to practical systems, such as fixed-wing unmanned aerial vehicles [52]. Finally, the study will further explore the application of event-triggered mechanisms in hypersonic flight vehicles [53].

Acknowledgments

This work was supported by the Shandong Provincial Natural Science Foundation, China (No. ZR2020QF055).

Conflicts of Interest

The authors declare no conflicts of interest.

Data Availability Statement

Data sharing is not applicable to this article as no datasets were generated or analyzed during the current study.

References

1. Z. J. Wu, X. J. Xie, and S. Y. Zhang, "Adaptive Backstepping Controller Design Using Stochastic Small-Gain Theorem," *Automatica* 43, no. 4 (2007): 608–620, https://doi.org/10.1016/j.automatica.2006.10.020.

2. F. Z. Gao, F. S. Yuan, and Y. Q. Wu, "Adaptive Stabilization for a Class of Stochastic Nonlinearly Parameterized Nonholonomic Systems With Unknown Control Coefficients," *Asian Journal of Control* 16, no. 6 (2014): 1829–1838, https://doi.org/10.1002/asjc.814.

3. L. Liu, Y. J. Liu, A. Chen, S. Tong, and C. P. Chen, "Integral Barrier Lyapunov Function-Based Adaptive Control for Switched Nonlinear Systems," *Science China Information Sciences* 63 (2020): 1–14, https://doi.org/10.1007/s11432-019-2714-7.

4. Y. M. Li, L. Liu, and G. Feng, "Robust Adaptive Output Feedback Control to a Class of Non-triangular Stochastic Nonlinear Systems," *Automatica* 89 (2018): 325–332, https://doi.org/10.1016/j.automatica.2017.12.020.

5. T. Wang, S. C. Tong, and Y. M. Li, "Robust Adaptive Decentralized Fuzzy Control for Stochastic Large-Scale Nonlinear Systems With Dynamical Uncertainties," *Neurocomputing* 97 (2012): 33–43, https://doi.org/10.1016/j.neucom.2012.05.017.

6. L. D. Fang, S. H. Ding, J. H. Park, and L. Ma, "Adaptive Fuzzy Output-Feedback Control Design for a Class of p-Norm Stochastic Nonlinear Systems With Output Constraints," *IEEE Transactions on Circuits and Systems I: Regular Papers* 68, no. 6 (2021): 2626–2638, https://doi.org/10.1109/TCSI.2021.3063084.

7. J. Wu, X. M. Chen, Q. J. Zhao, J. Li, and Z. G. Wu, "Adaptive Neural Dynamic Surface Control With Prespecified Tracking Accuracy of Uncertain Stochastic Nonstrict-Feedback Systems," *IEEE Transactions on Cybernetics* 52, no. 5 (2022): 3408–3421, https://doi.org/10.1109/TCYB.2020.3012607.

8. T. T. Gao, Y. J. Liu, D. P. Li, S. C. Tong, and T. S. Li, "Adaptive Neural Control Using Tangent Time-Varying BLFs for a Class of Uncertain Stochastic Nonlinear Systems With Full State Constraints," *IEEE Transactions on Cybernetics* 51, no. 4 (2021): 1943–1953, https://doi.org/10.1109/TCYB.2019.2906118.

9. L. Liu, X. S. Li, Y. J. Liu, and S. C. Tong, "Neural Network Based Adaptive Event Trigger Control for a Class of Electromagnetic Suspension Systems," *Control Engineering Practice* 106 (2021): 104675, https://doi.org/10.1016/j.conengprac.2020.104675.

10991239, 2025, 6, Downloaded from https://onlinelibrary.wiley.com/doi/10.1002/rnc.7799 by QINGDAO UNIVERSITY OF SCIENCE & TECH, Wiley Online Library on [04/03/2026]. See the Terms and Conditions (https://onlinelibrary.wiley.com/terms-and-conditions) on Wiley Online Library for rules of use; OA articles are governed by the applicable Creative Commons License

10. W. J. He, S. L. Zhu, N. Li, and Y. Q. Han, "Adaptive Finite-Time Control for Switched Nonlinear Systems Subject to Multiple Objective Constraints via Multi-Dimensional Taylor Network Approach," *ISA Transactions* 136 (2024): 323–333, https://doi.org/10.1016/j.isatra.2022.10.048.

11. W. J. He, S. L. Zhu, L. T. Lu, and Y. Q. Han, "A Novel Network-Based Adaptive Fault-Tolerant Control of Switched Nonlinear Systems Subject to Multiple Faults Under Prescribed Performance," *ISA Transactions* 145 (2024): 78–86, https://doi.org/10.1016/j.isatra.2023.12.008.

12. Y. Q. Han and J. J. Sun, "Adaptive Finite-Time Control for a Class of Stochastic Nonlinear Systems With Input Saturation Constraints: A New Approach Based on Multi-Dimensional Taylor Network," *International Journal of Robust and Nonlinear Control* 34, no. 8 (2024): 5329–5345, https://doi.org/10.1002/rnc.7266.

13. L. T. Lu, S. L. Zhu, D. M. Wang, and Y. Q. Han, "Predefined-Time Adaptive Consensus Control for Nonlinear Multi-Agent Systems With Input Quantization and Actuator Faults," *Nonlinear Dynamics* 112 (2024): 14215–14234, https://doi.org/10.1007/s11071-024-09818-y.

14. Y. X. Li, "Barrier Lyapunov Function-Based Adaptive Asymptotic Tracking of Nonlinear Systems With Unknown Virtual Control Coefficients," *Automatica* 121 (2020): 109181, https://doi.org/10.1016/j.automatica.2020.109181.

15. Y. Wu, X. J. Xie, and Z. G. Hou, "Adaptive Fuzzy Asymptotic Tracking Control of State-Constrained High-Order Nonlinear Time-Delay Systems and Its Applications," *IEEE Transactions on Cybernetics* 52, no. 3 (2022): 1671–1680, https://doi.org/10.1109/TCYB.2020.2985707.

16. N. Pang, X. Wang, and Z. M. Wang, "Observer-Based Event-Triggered Adaptive Control for Nonlinear Multiagent Systems With Unknown States and Disturbances," *IEEE Transactions on Neural Networks and Learning Systems* 34, no. 9 (2023): 6663–6669, https://doi.org/10.1109/TNNLS.2021.3133440.

17. Y. Shi, X. L. Shao, W. Yang, and W. D. Zhang, "Event-Triggered Output Feedback Control for MEMS Gyroscope With Prescribed Performance," *IEEE Access* 8 (2020): 26293–26303, https://doi.org/10.1109/ACCESS.2020.2971018.

18. H. Q. Wang, K. Xu, and J. B. Qiu, "Event-Triggered Adaptive Fuzzy Fixed-Time Tracking Control for a Class of Nonstrict-Feedback Nonlinear Systems," *IEEE Transactions on Circuits and Systems I: Regular Papers* 68, no. 7 (2021): 3058–3068, https://doi.org/10.1109/TCSI.2021.3073024.

19. W. Q. Xu, X. P. Liu, H. Q. Wang, and Y. C. Zhou, "Event-Triggered Adaptive NN Tracking Control for MIMO Nonlinear Discrete-Time Systems," *IEEE Transactions on Neural Networks and Learning Systems* 33, no. 12 (2022): 7414–7424, https://doi.org/10.1109/TNNLS.2021.3084965.

20. Z. Liu, J. H. Wang, C. L. P. Chen, and Y. Zhang, "Event Trigger Fuzzy Adaptive Compensation Control of Uncertain Stochastic Nonlinear Systems With Actuator Failures," *IEEE Transactions on Fuzzy Systems* 26, no. 6 (2018): 3770–3781, https://doi.org/10.1109/TFUZZ.2018.2848909.

21. P. Tabuada, "Event-Triggered Real-Time Scheduling of Stabilizing Control Tasks," *IEEE Transactions on Automatic Control* 52, no. 9 (2007): 1680–1685, https://doi.org/10.1109/TAC.2007.904277.

22. J. K. Sun, J. Yang, S. H. Li, and W. X. Zheng, "Output-Based Dynamic Event-Triggered Mechanisms for Disturbance Rejection Control of Networked Nonlinear Systems," *IEEE Transactions on Cybernetics* 50, no. 5 (2020): 1978–1988, https://doi.org/10.1109/TCYB.2018.2877413.

23. Y. L. Wang, C. C. Lim, and P. Shi, "Adaptively Adjusted Event-Triggering Mechanism on Fault Detection for Networked Control Systems," *IEEE Transactions on Cybernetics* 47, no. 8 (2017): 2299–2311, https://doi.org/10.1109/TCYB.2016.2631903.

24. L. T. Xing, C. Y. Wen, Z. T. Liu, H. Y. Su, and J. P. Cai, "Event-Triggered Adaptive Control for a Class of Uncertain Nonlinear Systems," *IEEE Transactions on Automatic Control* 62, no. 4 (2017): 2071–2076, https://doi.org/10.1109/TAC.2016.2594204.

25. H. H. Pan, D. Zhang, W. C. Sun, and X. H. Yu, "Event-Triggered Adaptive Asymptotic Tracking Control of Uncertain MIMO Nonlinear Systems With Actuator Faults," *IEEE Transactions on Cybernetics* 52, no. 9 (2022): 8655–8667, https://doi.org/10.1109/TCYB.2021.3061888.

26. X. Y. Hu, Y. X. Li, S. C. Tong, and Z. S. Hou, "Event-Triggered Adaptive Fuzzy Asymptotic Tracking Control of Nonlinear Pure-Feedback Systems With Prescribed Performance," *IEEE Transactions on Cybernetics* 53, no. 4 (2023): 2380–2390, https://doi.org/10.1109/TCYB.2021.3118835.

27. X. Y. Hu, Y. X. Li, Z. S. Hou, and B. Niu, "Event-Triggered Prescribed Performance Adaptive Fuzzy Asymptotic Tracking of Nonstrict-Feedback Nonlinear Systems," *International Journal of Robust and Nonlinear Control* 31, no. 12 (2021): 5776–5795, https://doi.org/10.1002/rnc.5569.

28. Y. X. Li, X. Y. Hu, W. W. Che, and Z. S. Hou, "Event-Based Adaptive Fuzzy Asymptotic Tracking Control of Uncertain Nonlinear Systems," *IEEE Transactions on Fuzzy Systems* 29, no. 10 (2021): 3003–3013, https://doi.org/10.1109/TFUZZ.2020.3010643.

29. Z. Li, F. Wang, and J. H. Wang, "Adaptive Finite-Time Neural Control for a Class of Stochastic Nonlinear Systems With Known Hysteresis," *IEEE Access* 8 (2020): 123639–123648, https://doi.org/10.1109/ACCESS.2020.2974871.

30. C. Fu, Q. G. Wang, J. P. Yu, and C. Lin, "Neural Network-Based Finite-Time Command Filtering Control for Switched Nonlinear Systems With Backlash-Like Hysteresis," *IEEE Transactions on Neural Networks and Learning Systems* 32, no. 7 (2021): 3268–3273, https://doi.org/10.1109/TNNLS.2020.3009871.

31. Y. J. Liu, S. C. Tong, C. L. P. Chen, and D. J. Li, "Neural Controller Design-Based Adaptive Control for Nonlinear MIMO Systems With Unknown Hysteresis Inputs," *IEEE Transactions on Cybernetics* 46, no. 1 (2016): 9–19, https://doi.org/10.1109/TCYB.2015.2388582.

32. G. Z. Cui, J. P. Yu, and Q. G. Wang, "Finite-Time Adaptive Fuzzy Control for MIMO Nonlinear Systems With Input Saturation via Improved Command-Filtered Backstepping," *IEEE Transactions on Systems, Man, and Cybernetics: Systems* 52, no. 2 (2022): 980–989, https://doi.org/10.1109/TSMC.2020.3010642.

33. H. T. Zhu, X. D. Li, and S. J. Song, "Input-To-State Stability of Nonlinear Impulsive Systems Subjects to Actuator Saturation and External Disturbance," *IEEE Transactions on Cybernetics* 53, no. 1 (2023): 173–183, https://doi.org/10.1109/TCYB.2021.3090803.

34. K. Xie, Z. L. Lyu, Z. Liu, Y. Zhang, and C. L. P. Chen, "Adaptive Neural Quantized Control for a Class of MIMO Switched Nonlinear Systems With Asymmetric Actuator Dead-Zone," *IEEE Transactions on Neural Networks and Learning Systems* 31, no. 6 (2020): 1927–1941, https://doi.org/10.1109/TNNLS.2019.2927507.

35. Z. Liu, F. Wang, Y. Zhang, X. Chen, and C. L. P. Chen, "Adaptive Tracking Control for a Class of Nonlinear Systems With a Fuzzy Dead-Zone Input," *IEEE Transactions on Fuzzy Systems* 23, no. 1 (2015): 193–204, https://doi.org/10.1109/TFUZZ.2014.2310491.

36. T. P. Zhang and S. S. Ge, "Adaptive Neural Control of MIMO Nonlinear State Time-Varying Delay Systems With Unknown Dead-Zones and Gain Signs," *Automatica* 43, no. 6 (2007): 1021–1033, https://doi.org/10.1016/j.automatica.2006.12.014.

37. J. H. Wang, Z. Liu, C. L. P. Chen, and Y. Zhang, "Event-Triggered Neural Adaptive Failure Compensation Control for Stochastic Systems With Dead-Zone Output," *Nonlinear Dynamics* 96 (2019): 2179–2196, https://doi.org/10.1007/s11071-019-04916-8.

38. Z. Namadchian and M. Rouhani, "Adaptive Prescribed Performance Neural Network Control for Switched Stochastic Pure-Feedback Systems With Unknown Hysteresis," *Neurocomputing* 429 (2021): 151–165, https://doi.org/10.1016/j.neucom.2020.11.044.

39. Y. Wu, H. Ma, M. Chen, and H. Y. Li, "Observer-Based Fixed-Time Adaptive Fuzzy Bipartite Containment Control for Multi-Agent Systems

10991239, 2025, 6, Downloaded from https://onlinelibrary.wiley.com/doi/10.1002/rnc.7799 by QINGDAO UNIVERSITY OF SCIENCE & TECH, Wiley Online Library on [04/03/2026]. See the Terms and Conditions (https://onlinelibrary.wiley.com/terms-and-conditions) on Wiley Online Library for rules of use; OA articles are governed by the applicable Creative Commons License

With Unknown Hysteresis," *IEEE Transactions on Fuzzy Systems* 30, no. 5 (2022): 1302–1312, https://doi.org/10.1109/TFUZZ.2021.3057987.

40. T. Yu, L. Ma, and H. W. Zhang, "Prescribed Performance for Bipartite Tracking Control of Nonlinear Multiagent Systems With Hysteresis Input Uncertainties," *IEEE Transactions on Cybernetics* 49, no. 4 (2019): 1327–1338, https://doi.org/10.1109/TCYB.2018.2800297.

41. Z. Liu, G. Y. Lai, Y. Zhang, X. Chen, and C. L. P. Chen, "Adaptive Neural Control for a Class of Nonlinear Time-Varying Delay Systems With Unknown Hysteresis," *IEEE Transactions on Neural Networks and Learning Systems* 25, no. 12 (2014): 2129–2140, https://doi.org/10.1109/TNNLS.2014.2305717.

42. L. Wang, W. Sun, and Y. Q. Wu, "Adaptive Asymptotic Tracking Control for Stochastic Nonlinear Systems With Unknown Backlash-Like Hysteresis," *Journal of Systems Science and Complexity* 35, no. 5 (2022): 1824–1838, https://doi.org/10.1007/s11424-022-1111-y.

43. Y. Sun, P. Shi, and C. C. Lim, "Event-Triggered Adaptive Leaderless Consensus Control for Nonlinear Multi-Agent Systems With Unknown Backlash-Like Hysteresis," *International Journal of Robust and Nonlinear Control* 31, no. 15 (2021): 7409–7424, https://doi.org/10.1002/rnc.5692.

44. K. X. Lu, Z. Liu, C. L. P. Chen, and Y. Zhang, "Event-Triggered Neural Control of Nonlinear Systems With Rate-Dependent Hysteresis Input Based on a New Filter," *IEEE Transactions on Neural Networks and Learning Systems* 31, no. 4 (2020): 1270–1284, https://doi.org/10.1109/TNNLS.2019.2919641.

45. D. B. Liu, Y. Fang, and H. B. Wang, "Intelligent Rate-Dependent Hysteresis Control Compensator Design With Bouc-Wen Model Based on RMSO for Piezoelectric Actuator," *IEEE Access* 8 (2020): 63993–64001, https://doi.org/10.1109/ACCESS.2020.2984645.

46. S. L. Xiao and Y. M. Li, "Modeling and High Dynamic Compensating the Rate-Dependent Hysteresis of Piezoelectric Actuators via a Novel Modified Inverse Preisach Model," *IEEE Transactions on Control Systems Technology* 21, no. 5 (2013): 1549–1557, https://doi.org/10.1109/TCST.2012.2206029.

47. D. M. Wang, Y. Q. Han, L. T. Lu, and S. L. Zhu, "Dynamic Event-Triggered Adaptive Tracking Control for Stochastic Nonlinear Systems With Deferred Time-Varying Constraints," *Chaos, Solitons & Fractals* 182 (2024): 114814, https://doi.org/10.1016/j.chaos.2024.114814.

48. M. X. Wang, S. L. Zhu, S. M. Liu, Y. Du, and Y. Q. Han, "Design of Adaptive Finite-Time Fault-Tolerant Controller for Stochastic Nonlinear Systems With Multiple Faults," *IEEE Transactions on Automation Science and Engineering* 20, no. 4 (2023): 2492–2502, https://doi.org/10.1109/TASE.2022.3206328.

49. Y. Du, S. L. Zhu, L. L. Zhai, and Y. Q. Han, "Switching Threshold-Based Event-Triggered Adaptive Asymptotic Tracking Control for Stochastic Nonlinear Systems With Full-State Constraints," *International Journal of Robust and Nonlinear Control* 33, no. 13 (2023): 7908–7928, https://doi.org/10.1002/rnc.6803.

50. L. J. Wang and C. L. P. Chen, "Reduced-Order Observer-Based Dynamic Event-Triggered Adaptive NN Control for Stochastic Nonlinear Systems Subject to Unknown Input Saturation," *IEEE Transactions on Neural Networks and Learning Systems* 32, no. 14 (2021): 1678–1690, https://doi.org/10.1109/TNNLS.2020.2986281.

51. M. L. Lv and N. Wang, "Distributed Control for Uncertain Multi-Agent Systems With the Powers of Positive-Odd Numbers: A Low-Complexity Design Approach," *IEEE Transactions on Automatic Control* 69, no. 1 (2024): 434–441, https://doi.org/10.1109/TAC.2023.3266986.

52. M. L. Lv, C. K. Ahn, B. Y. Zhang, and A. Q. Fu, "Fixed-Time Anti-Saturation Cooperative Control for Networked Fixed-Wing Unmanned Aerial Vehicles Considering Actuator Failures," *IEEE Transactions on Aerospace and Electronic Systems* 59, no. 6 (2023): 8812–8825, https://doi.org/10.1109/TAES.2023.3311420.

53. M. L. Lv, C. K. Ahn, P. Wang, R. W. Zuo, and J. D. Cao, "Event-Based Distributed Bipartite Consensus of High-Order Nonlinear Multi-Agent Network: Applications to Hypersonic Flight Vehicles," *IEEE Transactions on Automation Science and Engineering* (2024), https://doi.org/10.1109/TASE.2024.3408650.

10991239, 2025, 6, Downloaded from https://onlinelibrary.wiley.com/doi/10.1002/rnc.7799 by QINGDAO UNIVERSITY OF SCIENCE & TECH, Wiley Online Library on [04/03/2026]. See the Terms and Conditions (https://onlinelibrary.wiley.com/terms-and-conditions) on Wiley Online Library for rules of use; OA articles are governed by the applicable Creative Commons License